2D NUMERICAL SIMULATION OF VESSELS ADVANCING IN LEVEL ICE AND ICE MANAGEMENT OPERATIONS

by

© Ahmed Hassanin, B.Sc.

A thesis submitted to the School of Graduate Studies

in partial fulfillment of the requirements for the degree of

Master of Engineering

Faculty of Engineering and Applied Science

Memorial University of Newfoundland

May 2023

St. John's Newfoundland and Labrador Canada

Abstract

This thesis provides a hybrid, numerical and semi-empirical model that predicts ship-ice interaction in level ice. In addition, the model is integrated into an existing software solution, allowing for the simulation of ice management operations and vessel control in sea ice environments. The software implementation numerically solves for contact surfaces between the ship and ice in the time domain and utilizes semi-empirical formulas to estimate the ice forces generated in the interaction. A new method that does not remove rubble ice from the simulation is proposed. The addition of broken ice floes and increased ice shape complexity is facilitated by applying polygon partitioning and simplification algorithms to allow for a an adjustable trade-off between accuracy and performance. The software solution is validated using the data from model-scale tests and-full scale trials. Finally, recommendations for future work to improve upon the proposed model are provided.

Acknowledgments

I want to express my sincere gratitude to my supervisor, Dr. Dennis Peters, and my co-supervisors, Dr. Claude Daley and Dr. Brue Quinton. Their continuous guidance and support were crucial for me to be able to continue my studies even during the COVID-19 global pandemic. Further, I graciously acknowledge the financial support from the NSERC DND/CRD "Operational Capabilities of Low- and Non-ice-class Structures in Ice" grant, and the following contributing project partners: Defence Research and Development Canada (Atlantic), Vard Marine Inc., the American Bureau of Shipping (ABS), and the Newfoundland & Labrador Provincial Government's Department of Industry, Energy and Technology. I am thankful to Quan Zhou for his assistance with inquiries regarding his work. I would also like to thank Lori Hogan for her constant support during my studies and teaching assistant work. Last and far from least, I would like to express thanks to the friends and family I met during my studies and their support throughout this journey. I specifically extend my gratitude to my generous neighbours, Alex, Melanie, Emilio, and Kay; my first friends on the island, Farah, Hanya, Lore, Domé, Cleo, and Kathrine; and to the overall wonderful beings, Nour, Lexx, Tania, Stephen, Kristen, Ash, Vanessa, Sara, Kerri, Lea, Robert, Jackie, Sal, Rhys, Viv, Natasha, Andre, Anne, Jenne, Jess, Madison, Kassie, Krys, Kate, Katie, and the many others who made me feel at home after moving half-way across the world.

Table of Contents

List of Tables

List of Figures

List of Symbols or Abbreviations

A_{cr}	Area of the contact surface
B, T, L	Breadth, draft, and length of the ship at the waterline
C_f, C_l, C_v, C_{mid}	Tunable empirical coefficients
D	Flexural rigidity of the ice plate
DOF	Degrees of freedom
E	Young's modulus of ice
F_E, F_H	Environmental, Hydrodynamic forces and moment vectors
F_P, F_R	Propeller, Rudder force and moment vectors
F_{WT}, F_{WD}	Water-induced, Wind-induced force and moment vector s
$F_{cr,v}$	Vertical crushing force responsible for ice plate deflection
F_{cr}, F_{br}, F_{sb}	Ice crushing, breaking, submergence force and moment vectors
F_{ice}	Ice-induces force and moment vector
F_{total}	Total rigid body force and moment vector
f_h, f_v	Horizontal and vertical ice crushing force components
GEM	GPU-Event-Mechanics

g	Acceleration due to gravity
h_i	Ice thickness
L_h, L_c	Width and penetration of the contact geometry
L_{stern}, L_{bow}	Length of the stern and the bow
l_c	Characteristic length of the ice plate
P_{ave}	Average pressure on the contact surface
P_{flex}	Bearing capacity of the ice plate
p_0	Ice crushing strength
R_{ice}	Total level ice resistance experienced by a ship
R_s	Ice submergence resistance
v	Vessel speed
$v_{n,1}$	Normal velocity tangential to the contact surface
$v_{n,2}$	Relative velocity component normal to the contact surface
v_{sway}, v_{surge}	Ship velocity in the sway and surge directions
v_τ	Tangential component of relative velocity
w_0	Deflection at the apex of a semi-infinite plate
X_{br}, Y_{br}, N_{br}	x, y, and yaw moment components of the ice breaking force

$X_{ice}, Y_{ice}, N_{ice}$	x, y, and yaw moment components of the ice-induced force
X_{sb}, Y_{sb}, N_{sb}	x, y, and yaw moment components of the submergence force
$Y_{sb,bow}, Y_{sb,mid}$	Sway force at the bow and midship
α	Waterline angle
$\bar{\alpha}$	Average sheer angle over the bow sides
β'	Normal frame angle
γ	Sheer (buttock) angle
$\bar{\gamma}$	Average waterline angle over the bow sides
$\delta_s, \delta_s, \delta_c$	Crushing vertical displacement, flexural deflection, and penetration
μ	Friction coefficient between the ice and the ship.
ν	Poisson's ratio
ρ_Δ	The difference in density between water and ice
ρ_i, ρ_w	Density of ice and density of water
σ_f	Flexural strength of ice

Chapter 1: Introduction

The reducing extent of sea ice cover in the Arctic region during recent years makes it possible to increase ship traffic across the Arctic and Sub-Arctic regions and significantly reduce the length of shipping routes, namely those between Europe and East Asia. However, sea ice can pose a significant risk to the structural integrity of ships as the ship-ice interaction can generate substantial force. This ice force manifests as resistance to the motion of ice-going vessels. The resistance experienced in ice may far exceed that of open water. Therefore, accurately estimating the resistance force is essential to determine the required engine power and safety constraints of ice-going ships, most notably, icebreakers.

It is not always feasible to fit ships with more powerful engines and reinforced hulls in order to counteract the forces generated by sea ice. Therefore, through specialized ice breakers, ice management is used to allow less powerful vessels to traverse ice-covered waters with minimal risk. Ice breakers with a sufficiently high ice class can open a channel in the level ice (Fig. 5.8) that primarily contains small rubble ice pieces. Consequently, the ice resistance experienced by a vessel in a broken channel is significantly reduced, allowing access for vessels with lower ice classes. Ice management is repeatedly overlooked in the research concerned with level ice breaking despite its practical applications. Assessing the effectiveness of ice management plans is vital for successful operation in sea ice environments.

1.1 Background

According to Jones [1], the first scientific paper on ice breakers attempting to estimate level ice resistance was by Runeberg [2]. Due to the increased interest in oil and resource exploration in Arctic and Atlantic oceans, extensive research on ice resistance was conducted beginning in the 1960s. One of the significant advances in this topic was performed by Enkvist [3] who analytically divided level ice resistance into an ice breaking term, a submersion term, and a velocity-dependent term. Other significant studies during this period were [4]–[9]. These works resulted in several level ice resistance models based on physical modelling, model-scale tests, and full-scale tests. Due to the increase in available computational power, the 21st century witnessed the development of several ice breaking numerical models such as the models in [10]–[13], and less focus was given to analytical solutions.

Ice breaking resistance is a complex problem that includes solid-solid and solid-fluid interaction. To model this level of complexity, a few assumptions and simplifications are generally accepted. The most common one is splitting the total ice resistance into multiple components that can be effectively isolated and measured. This assumption is often found in models presented in [3]–[6], [8], [9], [14]. According to Zhou et al. [13], based on the work of Spencer et al. [14], the total ice resistance affecting a ship manoeuvring in level ice consists of three major components: ice breaking, ice clearing, and ice buoyancy. However, other work, such as [15] considers the three components to be ice breaking, ice rotation, and ice submersion. Most models agree on the importance of ice breaking and ice submersion while being less confident of the contribution of other processes, such as ice rotation.

In ice breaking, the movement of the ship into an ice sheet causes the crushing of the edge of the sheet with local crushing and shear failure. The stress within the ice sheet keeps building

up until it exceeds the flexural limit of the sheet. This leads to bending failure and the formation of a crack, resulting in an ice piece breaking off the ice sheet, as shown in Fig. 1.1. According to Valanto [16], ice rotation starts after an ice piece has broken off. Due to the relative motion between the ship and ice, the broken ice piece is accelerated by the hull and rotated until it is parallel to the hull. The rotation ends with the ice piece impacting the hull, causing it to stop rotating [15]. In the submersion process, the broken ice pieces slide along the hull of the ship until they leave the body of the ship.

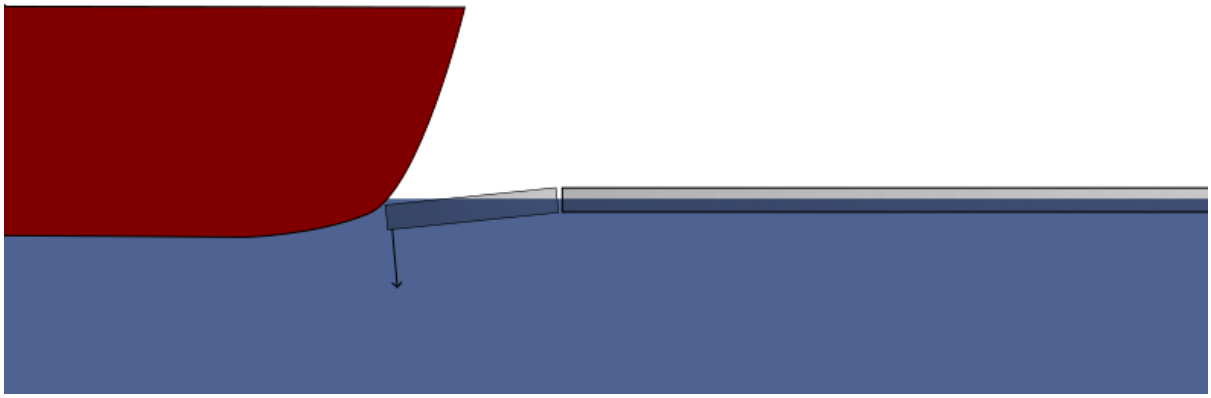

Fig. 1.1. An ice piece breaking off the ice sheet due to bending failure.

The ice breaking process is the most extensively modelled component in literature, with both analytical and numerical solutions developed. This includes the modelling of ice crushing, shearing, and bending failure. There are numerical ice crushing models such as [17], [18]. However, bending failure solutions for global-scale ship performance models tend to use simplified analytical approaches such as the breaking formula in [8]. Simplified analytical techniques are preferred as numerically modelling the process is computationally expensive, often requiring continuum methods such as Finite Element Method (FEM).

There is not much work exploring the effect of ice rotation (Fig. 1.2) in the literature. In fact, some models [8], [11], [13] entirely neglect the ice rotation resistance while still maintaining a

reasonable estimation of total level ice resistance [15]. Therefore, the importance of ice rotation in ice resistance models is still not evident. Most of the work on ice rotation resistance was conducted by Valanto [10], [16], [19] in a series of experiments and theoretical models. Valanto concluded that ice rotation participates in a significant portion of the total ice resistance, almost equal to that of ice breaking. Some other prominent models that explored the effect of ice rotation resistance are [3], [7], [20], [21]. In contrast to ice breaking, where several numerical models have been developed, ice submersion models such as [3], [7], [8], [14] are largely analytical solutions with semi-empirical coefficients.

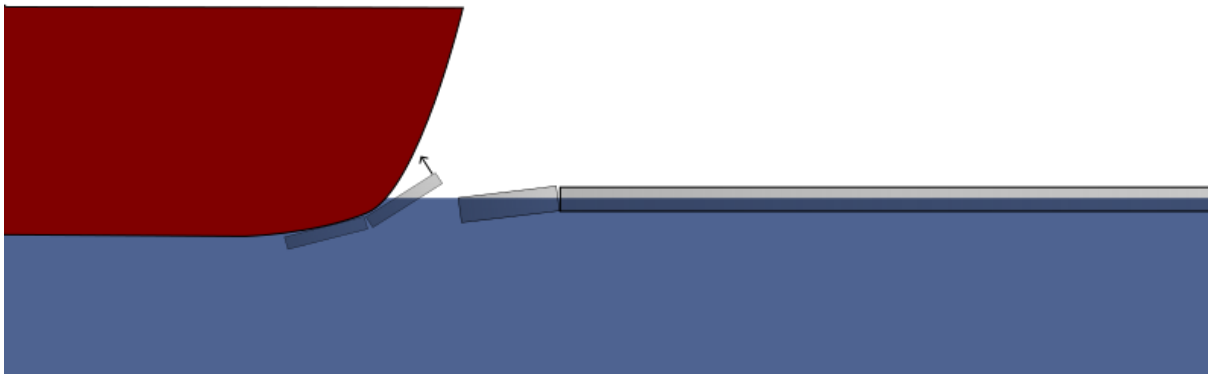

Fig. 1.2. An ice piece rotating towards the hull of the ship after breaking off the ice sheet.

1.2 Numerical Solutions

Due to the high cost of model testing, numerical modelling is more valuable in optimizing ship design. Aside from the upfront development time of the numerical model, numerical experiments take considerably less time to conduct than model tests. Numerical models also tend to provide more accurate results compared to analytical models, as analytical models attempt to find the average solution over the entire process. In contrast, numerical models work

on shorter intervals providing an accurate solution at each position in space and for each time interval.

There is much uncertainty regarding ice properties such as thickness, strength, and friction in real-world experiments. This uncertainty makes it difficult to determine which factors affect the ice loads experienced by a ship. Therefore, numerical models make strict assumptions about ice geometry, mechanical properties, hydrodynamics, and environmental forces. The physical interaction is variable in nature, particularly when it comes to ice geometry and mechanical properties. However, these assumptions are necessary as it is challenging to record ice behaviour, not to mention the computational complexity from attempting to model a system with such high variability. Most of the existing ice breaking numerical models, such as [10], [11], [13], [20], [22], contain empirical solutions to compensate for the lack of complete models of ice mechanics [15].

As reviewed by Xue et al. [23], there are two main types of methods used to develop numerical ice models: Particle methods such as Discrete Element Method (DEM), The Smoothed Particle Hydrodynamics (SPH) method, and Peridynamics (PD). The other being Continuum methods such as FEM, Finite Difference Method (FDM), and Particle in Cell (PIC) method.

The advantage of continuum methods such as FEM is their high mathematical modelling accuracy on the microscale for problems such as contact collision, deformations, and fractures in the ice structure. Studies that focus on the interaction and forces between the hull and ice tend to use the FEM approaches for this reason. On the other hand, particle methods such as DEM tend to be employed in work concerned with dynamic discrete objects such as ice floes, crushed ice, and ship navigation and performance.

Out of the three particle methods mentioned, DEM has been extensively used in previous work, such as [13], [18], to describe the process of ship-ice interaction. This is due to the advantage

of DEM being able to describe the discrete cyclic events of ice breaking on the local scale and the forces affecting the interaction on the global scale. However, unlike continuum methods, DEM does not have a strict mathematical definition in contrast to the finite elements and element-level equations of FEM. Therefore, DEM often depends on special purpose solutions for the application in question.

A prominent disadvantage of numerical models is their high computational cost, which results in their inability to satisfy the constraints of real-time in operating environments. This is particularly the case of FEM, as it requires massive computational resources. DEM suffers from the same downside. However, DEM models can be engineered to sacrifice accuracy in exchange for a lower demand for computational resources, whereas FEM is more strict and is mainly employed for its computational accuracy. Due to the discrete, independent nature of DEM particles, DEM models tend to highly benefit from parallel data accelerators such as graphical processing units (GPUs) [23], resulting in significantly reduced execution time. Therefore, a variation on DEM was chosen as the method to model level ice breaking for the GPU-Event-Mechanics (GEM) tool with which this work is concerned.

1.3 GEM

GPU-Event-Mechanics (GEM) is a simulation tool for ship operations in sea ice developed by researchers at the Memorial University of Newfoundland. The work on GEM started as a part of the Sustainable Technology for Polar Ships and Structures (STePS2) project, which aimed to provide a better understanding of the sea ice - steel structure interaction and develop practical design tools for the assessment of vessel and offshore structure safety in sea ice environments. GEM is intended for use in voyage planning, ship design, ship safety evaluation, operator training, and real-time vessel control. GEM is meant to be lightweight, fast, and portable. It is

able to run open pack ice (Fig. 1.3) simulations in hyper-real-time on relatively affordable commercial hardware, making it possible to run simulations on ice-going vessels during operation. Furthermore, the hyper-real-time capability opens the gate for future real-time control by enabling live simulations through the use of AI to filter and annotate sensor data before feeding this information into GEM.

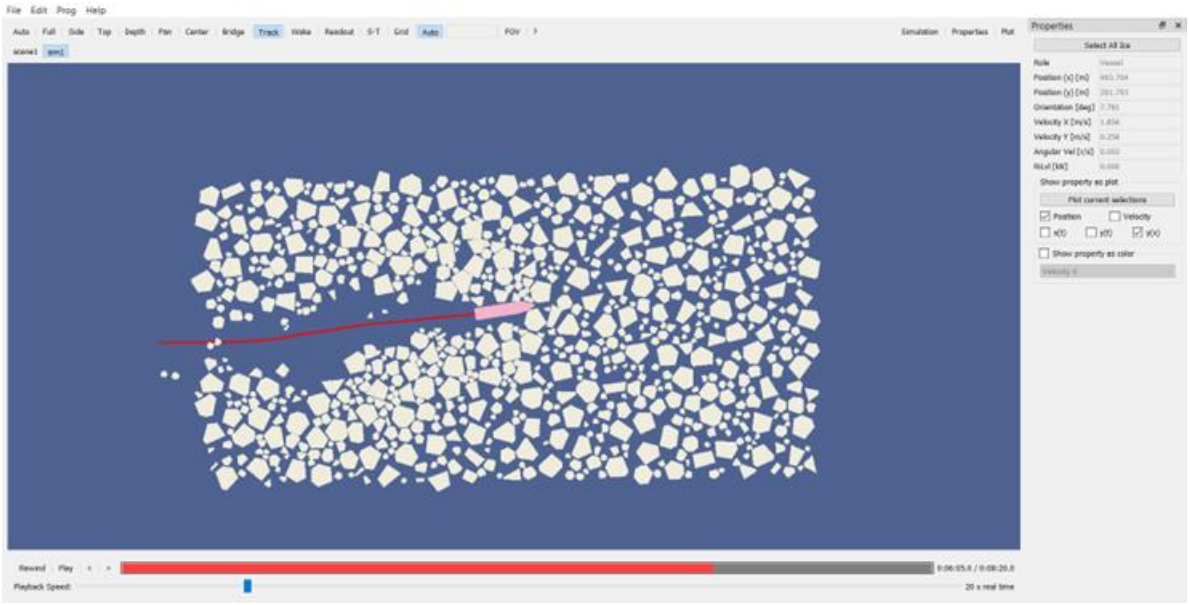

Fig. 1.3. Simulation playback of an open pack ice scene in GEM.

GEM is separated into two components, the physics kernel and the scene viewer. The physics kernel was developed in C/C++. It handles the calculations necessary to simulate everything in an ice scene, from ice impacts to vessel kinematics. The scene viewer was developed in C++ using the Qt framework [24] and OpenGL [25]. It builds 3D scenes out of the ice data frames generated by the physics kernel and uses them to stitch together a simulation video. It can also be used to create ice scenes and input parameters for the simulation. Fig. 1.3 shows a screenshot of an ice scene in the user interface of GEM.

At present, GEM is only able to simulate rigid bodies and discrete events. All vessels, structures, and ice floes within the simulation space are modelled as discrete ridgid bodies with simple properties. This is a part of an approach called the Ice Event Mechanics Modelling (IEMM) method, described in [26]. The IEMM approach considers the system mechanics to be only governed by a set of discrete contact and failure events described by simple analytical solutions such as the conservation of collision energy method [27] and simple 2D movement, hence the Event-Mechanics part of GPU-Event-Mechanics. IEMM is based on the premise that the behaviour of the system as a whole depends more on the sequence of interactions rather than any single event. IEMM also assumes that, relative to the interval between simulation timesteps, fracture and collision events happen in such a short time that they can be considered instant discrete events rather than continuous processes. The discreteness of GEM models coupled with the simple event solutions enables GEM to simulate a large system in hyper-real-time by utilizing the highly parallel nature of IEMM. A more detailed description of the pack ice model of GEM can be found in [26], [28], [29].

Currently, GEM can break the edges off ice floes in collision events. However, it does not support continuous level ice breaking. With fully integrated 2D level ice breaking, GEM will be able to give an accurate estimation of resistance in ice for different classes of vessels under various ice conditions. It will also enable the prediction of the hull impact loads during level ice breaking operations. In addition, more real-world ice management scenarios will be possible to simulate since sea ice conditions would not be restricted to pack ice only.

There are some challenges with adding level ice breaking to GEM. Most prominently, GEM only supports simulating ‘instant’ events between discrete objects; meanwhile, ice breaking is a continuous process that progresses over several timesteps. This type of continuous progression is not yet supported in GEM. Therefore, the level ice breaking feature will result

in refactoring a considerable portion of the codebase. Another crucial point is that adding a feature based on continuum mechanics to GEM will result in a reduction in simulation speed. Simulation speed is one of the most vital features of GEM. Adding level ice breaking without compromising the hyper-real-time simulation speed is a tricky problem that involves making the right assumptions and simplifications while still maintaining engineering accuracy. Another challenge is that the collision detection method mentioned in [26] is a general polygon overlap algorithm, which results in less code, less complicated collision scenarios, and faster execution. However, this algorithm alone is not able to accurately represent the concave polygons that might result from level ice breaking. These challenges are further explored in chapter 3.

1.4 Objectives

This research aims to develop a level ice breaking algorithm that can be integrated with the current open pack ice numerical model in the 2D simulation tool GEM. The new version of GEM should be capable of simulating both the process of continuous level ice breaking on the micro-scale and the interaction between the broken sea-ice pieces and vessels and, in extension, ice management operations on the macro scale.

The main objectives of this work are:

- To develop a numerical ship-ice interaction model that is able to accurately predict ice loads and level ice resistance in the time domain.

- To integrate the proposed model into the 2D pack ice simulation environment of GEM while preserving its hyper-real-time capability.

- To validate the model by comparing the new simulation environment's predictions to data from full-scale trials and model tests.

- To provide recommendations for possible future work building on this model.

1.5 Thesis Outline

- **Chapter 1** includes an introduction to this thesis; provides the necessary general background, research objectives, and scope of this work; and outlines the structure of the thesis presenting this work.

- **Chapter 2** presents a detailed literature review of previous work on mathematical and numerical modelling of ship-ice interaction; and explores the most promising analytical, semi-empirical, and numerical level ice breaking models for the purpose of this work.

- **Chapter 3** builds on chapter 2 to develop a continuous level ice breaking model and describes how it can be integrated into the current pack ice simulation environment of GEM.

- **Chapter 4** describes the implementation of the model developed in chapter 3.

- **Chapter 5** presents the results of several validation experiments conducted using the new simulation environment.

- **Chapter 6** concludes the current work and offers recommendations for future work.

Chapter 2: Literature Review

The resistance experienced by vessels in level ice has been explored extensively in the literature, notably with the increased traffic through the Arctic and Sub-Arctic in recent years. A couple of works have already provided a review of previous research on ice resistance [1], [23], [30]. They are a significant contributor to the information provided in this literature review. In this chapter, existing models were compiled and assessed based on their relevance for the purpose of developing a level ice breaking algorithm in GEM that leverages its speed while maintaining engineering accuracy.

2.1 Empirical Solutions

Before World War II, only one notable work included a detailed analysis of ice resistance. Shimanskii [31] proposed a semi-empirical method for investigating continuous mode ice breaking resistance. He developed the parameters of the equation. However, the coefficients were left to be deducted from full-scale experiments [1].

2.1.1 Jansson

The majority of the research on level ice breaking has been published after WWII, prompted by the rising oil prices and the first voyage of a commercial vessel through the Northwest Passage by the oil tanker SS Manhattan in 1969. One of the earliest works of this period that provided a model of level ice resistance was by Jansson [32]. Jansson discussed the history and science of ice breaking and quoted, without reference, values for the physical properties of freshwater ice [1].

He mentioned that he had not found reliable values for sea ice. However, he provided a simple formula for level ice resistance:

$$R_{ice} = (C_1 h_i + C_2 h_i v^2) B \qquad (1)$$

Where C_1 and C_2 are experimental constants, h_i is ice thickness (m), v is vessel speed (m/s), and B is the breadth of the vessel at the waterline (m).

2.1.2 Kashteljan et al

The first analytical solution that provided a formula where level ice resistance was broken into separate components was proposed by Kashteljan et al. [4]:

$$R_{TOT} = R_1 + R_2 + R_3 + R_4 \qquad (2)$$

Where R_1 is the ice breaking resistance; R_2 is the resistance connected to weight (i.e., submersion of broken ice, turning of broken ice, change of position of the vessel, and dry friction); R_3 is the resistance from moving through broken ice; and R_4 is the resistance due to water friction and wavemaking. The terms R_1, R_2, R_3 contained five empirical coefficients K_1, K_2, K_3, K_4, K_5 which were experimentally determined from the data of the full-scale tests of the Ermak.

2.1.3 Lewis and Edwards

Lewis and Edwards [5] later modified Kashteljan's formula based on a regression analysis of available test data and proposed the following:

$$R_{im} = C_o \sigma_f h_i^2 + C_1 \rho_i g B h_i^2 + C_2 \rho_i B h_i v^2 \qquad (3)$$

Where R_{im} is the mean ice resistance, σ_f is ice flexural strength (kPa), ρ_i is the density of ice (kg/m^3), g is the acceleration due to gravity (m/s^2), and C_1, C_2, C_3 are empirical coefficients

determined experimentally. The first term is for the ice breaking and friction resistance, the second term is for the ice buoyancy resistance, and the third term is for the resistance due to momentum exchange between the ship and the broken ice. C_1, C_2, C_3 were derived from the full-scale and model-scale tests of Wind-class, Raritan, M-9, and M-15.

2.1.4 Enkvist

The work of Enkvist [3] provided a significant contribution to the study of ship performance in level ice. He was able to isolate the velocity-dependent term of ice resistance by conducting tests at low speed and the submergence-dependent term by conducting tests in pre-sawn ice. This method of isolating the different components to assess their contribution to the total ice resistance has been the basis for the most promising models introduced in the literature in later work. He performed model-scale ice resistance tests for Moskva-class, Finncarrier, and Jelppari; and compared the results with data from the full-scale tests of these ships.

Further, he proposed a semi-empirical equation for level ice resistance based on these tests:

$$R_{TOT} = C_1 B h_i \sigma + C_2 B h_i T \rho_\Delta g + C_3 B h_i \rho_i v^2 \qquad (4)$$

Where T is the draft of the ship (m), and ρ_Δ is the difference in density between water and ice. Similar to [5], the first term is the resistance due to ice breaking, the second term is the resistance due to ice buoyancy, and the third term is the resistance due to momentum loss. However, Enkvist has emphasized the importance of the density difference between ice and water and the contribution of the draft of the ship to the ice buoyancy term. He later applied the same model-scale testing technique to 16 full-scale tests [33] concluding that the breaking term accounts for a significant portion of the total ice resistance experienced by a ship at low speeds. The contribution of ice breaking was estimated to be between 40% - 80% of the total resistance, with the larger value for smaller ships.

2.1.5 Milano

Milano [6] provided a new theoretical approach to predict performance in level ice based on the energy needed for a ship to be able to advance into the ice sheet. The total energy loss due to ship motion is written as:

$$E_T = E_1 + E_2 + E_3 + E_4 + E_5 \quad (5)$$

Where $E_1$is the energy lost due to moving through the ice-filled channel, E_2 is the energy absorbed through the local crushing of cusp wedges, E_3 is the energy needed to lift the ship onto the ice, E_4 is the energy that leads to ice fracture, and E_5 is the energy used to push the broken ice downwards. He derived an analytical solution for each of the above terms and compared the predictions of his model with the data from the Mackinaw, the Wind-class vessel Staten Island, and the Raritan. He found good correlation for thick ice and showed the dependence of ice resistance on vessel speed.

2.1.6 Kotras et al

Kotras et al. [7] proposed another semi-empirical approach based on the best fit of a portion of the data from Katmai Bay, Mackinaw, Radisson, Staten Island, and Manhattan. They gave the following expression, which showed good correlation with the rest of the data from these trials:

$$R_{ice} = R_B + R_{Bf} + R_T + R_{Tf} + R_S + R_{Sf} \quad (6)$$

Where R_{ice} is the total ice resistance the ship experiences (N), R_B is the normal ice breaking resistance, R_{Bf} is the frictional ice breaking resistance, R_T is the normal ice turning resistance, R_{Tf} is the frictional ice turning resistance, R_S is the normal ice submergence resistance, and R_{Sf} is the frictional ice submergence resistance. This work is one of the limited semi-empirical

solutions that explored the effect of rotation on the total ice resistance. There is also an emphasis on the importance of the contribution of friction to ice resistance.

2.1.7 Lindqvist

Lindqvist [8] proposed an analytical model that builds on previous work [3], [4], [33] to predict the ice resistance experienced by an ice-going ship. He assumed a sharp hull form that can be simplified as several flat plates. Daley [34] details the different components mentioned in the work of Lindqvist and provides the derivation for the formulas. An equation that approximates ice resistance in relation to the main principles of the ship, shown in Fig. 2.1, is given as:

$$R_{ice} = (R_c + R_B)\left(1 + 1.4\frac{v}{\sqrt{g.h}}\right) + R_S\left(1 + 9.4\frac{v}{\sqrt{g.L}}\right) \quad (7)$$

Where R_C is the resistance due to ice crushing at the stem, R_B is the resistance due to ice breaking, R_S is the resistance due to the submergence of the broken ice pieces, and L is the length of the ship (m).

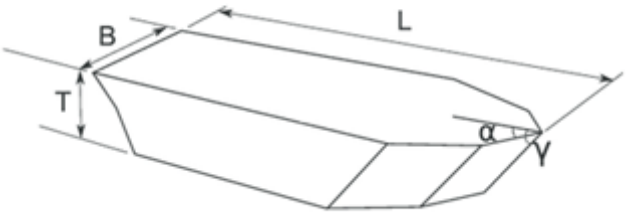

Fig. 2.1. Main ship principles as illustrated in [13].

For the ice crushing term R_C, Lindqvist starts with estimating the vertical force needed for an ice edge to reach flexural failure:

$$F_v = 0.5\ \sigma_f\ h_i^2 \tag{8}$$

Where F_v is the vertical force needed to fail an ice edge in flexural (N) and σ_f is the flexural strength of ice (MPa).

The crushing resistance the ship will experience is then given by:

$$R_c = F_v \frac{\tan(\gamma) + \mu \frac{\cos(\gamma)}{\cos(\psi)}}{1 - \mu \frac{\sin(\gamma)}{\cos(\psi)}} \tag{9}$$

$$\psi = \tan^{-1}\left(\frac{\tan(\gamma)}{\sin(\alpha)}\right) \tag{10}$$

Where α is the waterline angle at the stem, γ is the sheer (buttock) angle, and μ is the friction coefficient between the ice and the ship.

For the ice breaking term R_B, which is meant to express the average force (over time and in space) required to break the ice in flexure, the following equation is derived:

$$R_B = k.B\left(\frac{h_i^3}{l_c^2}\right)\left(\tan(\bar{\psi}) + \mu \frac{\cos(\bar{\gamma})}{\sin(\bar{\alpha})\cos(\bar{\psi})}\right)\left(1 + \frac{1}{\cos(\bar{\psi})}\right) \tag{11}$$

Where k is a constant, B is the beam of the ship; $\bar{\gamma}, \bar{\alpha}$ are the average waterline and sheer angles over the bow sides; and l_c is the characteristic length of the ice plate given by:

$$l_c = \left(\frac{E.h_i^3}{\rho_w.g.12(1-\nu^2)}\right)^{0.25} \tag{12}$$

E is Young's modulus of ice (kPa), ν is Poisson's ratio, and ρ_w is the density of sea water.

For the ice submergence term R_S, Lindqvist assumed that the bow is completely covered in broken ice, with only 70% of the rest of the hull getting covered in ice. According to [34], this

is not entirely accurate for all hull shapes and sizes. For example, some ships have features to clear the ice. The submergence resistance accounts for the force needed to sink the broken ice pieces and counteract the friction generated by ice sliding underneath the hull.

R_S is then given by:

$$R_S = \rho_\Delta . g . h_i . B \left(\frac{T(B+T)}{B+2T} + \mu \left(0.7L - \frac{T}{\tan(\bar{\gamma})} - 0.25 \frac{B}{\tan(\bar{\gamma})} + T \cos(\bar{\gamma}) \cos(\bar{\psi}) \sqrt{\frac{1}{\sin^2(\bar{\gamma}) + \frac{1}{\tan^2(\bar{\alpha})}}} \right) \right) \quad (13)$$

Finally, Lindqvist verified his formulas with the data from the Baltic Sea trails of three ships: Jelppari, Otso Kontio, and Vladivostok.

2.1.8 Colbourne

Colbourne [30] provided an extensive literature review of previous work on ice material properties and ice-induced forces. He proposed an analytical method to describe the ship-ice interaction based on model-scale tests in pre-sawn ice. Experiments in pre-sawn ice allowed him to isolate the ice breaking component of the resistance. He provided the following formulas

where non-dimensional numbers are used to be able to apply the method obtained from model-scale tests to full-scale date:

$$R_T = R_B + R_c + R_f \quad (14\ 1)$$

$$R_C = R_p(h_i, \rho, v) - R_f(v) \quad (15)$$

$$R_B = R_L(\sigma, h_i, \rho, v) - R_C(h_i, \rho, v) - R_f(v) \quad (16)$$

Where R_T is the total ice resistance; R_f is the viscous drag on the model calculated using the International Towing Tank Conference (ITTC) method; R_p is the pre-sawn ice resistance; R_c is the ice clearing resistance; R_L is the model resistance in level ice; and R_B is the resistance due to ice breaking. Colbourne then applied this method to the data collected from the full-scale tests of CCGS Louis S. St-Laurent, CCG R-Class Hull, MV Arctic, and USCGC Mobile Bay (WTGB-103).

2.1.9 Spencer et al

Spencer et al. [35] based their work on a similar regression model and model-scale testing system to that of Colbourne [30]. They split the total ice resistance into four components: an ice breaking component, an ice clearing component, a buoyancy component, and open water resistance. They also proposed a standardized testing and analysis procedure [36]. In later work, Spencer and Jones [14] applied this method to predict the level ice resistance of CCGS R-Class icebreakers and found good agreement between the calculated total resistance and measured resistance. The following expression for level ice resistance was given:

$$R_{tot} = R_w + R_{br} + R_{cl} + R_{bu} \quad (17)$$

Where R_w is the open water resistance, and R_{br}, R_{cl}, R_{bu} are the ice resistance due to ice breaking, ice clearing, and ice buoyancy, respectively.

Each ice resistance component is a regression formula that was derived from model tests and provided as:

$$R_{br} = C_{br}\rho_i B h_i v^2 \quad (18)$$

$$R_{cl} = C_{cl}F_h^{EX_{cl}}\rho_i B h_i v^2 \quad (19)$$

$$R_{bu} = C_{bu}\rho_\Delta g h_i B T \quad (20)$$

Where C_{br}, C_{cl}, C_b , and X_{cl} are empirical coefficients derived from model tests, and F_h is the Froude number of the ice given by:

$$F_h = \frac{v}{\sqrt{g h_i}} \quad (21)$$

2.1.10 Riska et al

Riska et. al [9] provided an analytical method that modified previous semi-empirical formulas such as [8] and derived a solution to ice resistance that can be written as:

$$R_i = C_1 + C_2 v \quad (22)$$

Where $C_1$and C_2 are functions of the main principles of the ship and ice thickness, and v modifies C_2 as the velocity-dependent term. The Finnish-Swedish Ice Class Rules (FSICR) adopted this method for calculating the level ice resistance of consolidated layers in an ice channel [15].

2.1.11 Summary

Although the work on empirical solutions and analytical models used different approaches, most of the published work seems to come to the same conclusion: Separating ice resistance into different components that could be isolated and tested independently simplifies the complex physical process. This allows for the development of otherwise unreasonable models that still provide predictions in good agreement with real-world data. Many numerical models also adopt this concept and employ some of the formulas provided in existing analytical solutions to simplify the numerical modelling of ship-ice interaction. Therefore, in this thesis, ice resistance will be separated into different components, and semi-empirical solutions will be integrated into the numerical solution to reduce modelling complexity.

2.2 Numerical Solutions

In the past three decades, with the advance of computation hardware, considerable efforts have been put into the development of numerical models of ice resistance. Most of these numerical models are based on the empirical formulas developed earlier. As mentioned in section 1.2, two main approaches are used to develop numerical ice models: Particle methods and Continuum methods. This section will mainly focus on Particle methods, specifically DEM, as it is the most relevant for the scope of this work. DEM partitions continuous materials into small discreet elements or objects that interact through pre-determined rules. It is extensively used in the numerical solutions for modeling ship-ice interactions [11], [13], [20], [22], [37]–[43].

2.2.1 Daley et al

Daley et al. [44] built on previous work [17] to propose a new conceptual model. The model describes ice failure as a nested hierarchy of discrete failure events where the geometry changes with each failure event, and consequently defines a subset of the initial conditions of the following failure event. This general concept easily lends itself to an iterative numerical model and thus was used by much of the early research into numerical simulations of structure-ice interaction.

2.2.2 Wang

Wang [43] was one of the works that adopted Daley's conceptual models. She simplified the model as a process of continuous ice crushing, bending, and rubble formation. She proposed a geometric grid method to simulate continuous contact between the structure and level ice. Analytical formulas are applied to attain crushing force and bearing capability. At the same time, a geometric grid method is used to numerically detect structure-ice contact and update the ice edge after flexural failure. She also assumed broken ice floes have a circular shape and gave an equation to calculate the size of broken ice pieces where their radius is a function of the speed of the ship and the characteristic length of ice.

2.2.3 Valanto

Valanto [10] proposed a numerical model to predict the forces on the waterline of a ship due to the ice breaking process. The predictions were compared with measurements from the MS Uisko and found good agreement between the prediction and the available data. He also calculated the ice resistance for several ships using a combination of his numerical model and

the semi-empirical model of Lindqvist [8] for the submergence component of the ice resistance. These estimates were also in good agreement with the measured values.

2.2.4 Lau et al

Lau et al. [45] proposed a numerical solution that considers the yaw moment induced by advancing into an ice sheet. They developed a model that decomposes the total yaw moment into hydrodynamic, breaking, submergence, and ice clearing components. Additionally, they derived an expression for the breaking and submergence components. The ice breaking force was simplified as three horizontal loads: Two acting on the bow and one on the bow shoulder facing the center of the turning circle. Yaw moment can then be obtained by multiplying those loads by the corresponding length to the ship's center of mass.

2.2.5 Sawamura et al

Sawamura et al. [40] developed a numerical method to calculate the repetitive ice breaking pattern and ice load on a ship advancing into a level sheet. In this method, the waterline of the ship and the ice plate are discretized into small circles, as illustrated in Fig. 2.2, which are used for contact detection. Contact occurs if the distance between the center of a ship circle and an ice edge circle is less than the sum of the radii of these circles. As the entire ice plate is discretized and tested for contact events, contact detection is relatively inefficient and could be optimized. Further, a Finite Element analysis of the fluid–ice interaction was used to examine the dynamic effect of bending failure on the ice breaking patterns. In later work, Sawamura [41] and Sawamura et al. [46] developed a numerical model to predict ship-ice interactions in broken ice floes. The calculated ice submerging force showed good agreement with experimental data. Sawamura et al. [47] developed a 2D numerical model to predict the ice breaking pattern and ice forces produced when an icebreaker advances into plate ice. The

calculated ice channel width and ice breaking resistance were compared with the measured resistance in the model test and showed good agreement.

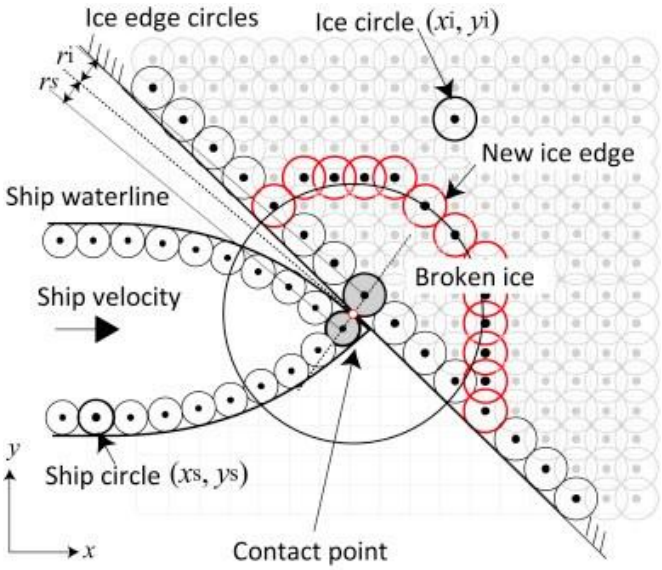

Fig. 2.2. Circle contact detection as illustrated in [42]

In his latest work, Sawamura [42] presented a 2D numerical method to model the ship-ice interaction of an icebreaker advancing into ice-covered water that includes both broken ice floes and an ice plate. The model simulates the repeated ice breaking of an ice plate and the removal of small ice floes. The same circle contact detection technique in [40] is used. The ice plate is broken in crushing, bending, and splitting mode. The ship-ice interaction in open pack ice is calculated using a physically-based model with rigid body equations in 3 Degrees Of Freedom (DOF). He concluded that the results of the method demonstrate how numerical simulations can be used to establish efficient ice management strategies. However, verification of the proposed numerical model is needed for future applications in ice management.

2.2.6 Nguyen et al

Nguyen et al. [38] proposed a mathematical model for simulating the behaviour of a dynamically-positioned ship operating in level ice. The ship-ice interaction is assumed to be a sequence of breaking events of an ice plate where each ice breaking event is a cycle of crushing and bending. In their work, only the ice edge and the waterline of the ship were discretized into points. Contact was determined based on the distance between two points, one was on the waterline of the ship, and the other was on the ice edge. They assumed that the ice crushing force increases linearly from zero to the value needed to break the ice edge in flexure. Thus, the force experienced by the ship can be calculated using the time interval since initial contact and the bearing capacity of the ice sheet. The ice resistance due to bending, submergence, and velocity dependence was calculated using the empirical formulas in [8].

2.2.7 Su et al

Su et al. [11] introduced a numerical method to simulate ship maneuvers in level ice. They followed the strategy of only discretizing the ice edge and the waterline of ship to reduce computational inefficiency. In contrast to Nguyen et al. [38], the ice crushing force is assumed to be proportional to the contact area, calculated numerically at each time step. Further, frictional forces and shoulder crushing were investigated. The frictional forces were added to the components of the ice crushing force and assumed to be proportional to the relative velocity components. The numerical model was validated using the full-scale data from the icebreaker AHTS/IB Tor Viking II, and good agreement was found.

2.2.8 Zhou and Peng

Zhou and Peng [48] further developed the model of Su et al. They presented a new DEM numerical model along with a different approach for contact detection that categorized possible ship-ice interactions into four scenarios (Fig. 2.3). In the contact detection method, the entire waterline of the ship is discretized while only the edge of the ice sheet is discretized as the ship is only able to interact with a limited section of the ice sheet per simulation iteration. A Point-In-Polygon approach is used to test for the ice nodes inside the polygon of the ship and for the ship nodes inside the ice sheet. In the first case, none of the points describing the waterline of the ship (black) are inside the polygon consisting of the sheet ice edge points (black) and the simulation boundaries. In the second case, there are ship waterline points inside the ice sheet polygon and ice sheet points inside the ship waterline polygon. In case three, none of the ship waterline points are inside the ice sheet polygon, but there are ice sheet points inside the ship waterline polygon. In case four, none of the ice nodes are inside the ship waterline polygon, but there are ship waterline points inside the ice sheet polygon.

In further work, Zhou et al. [13] expanded on their ship–ice interaction model. They proposed a method to make corrections for the change in contact area due to the deflection of the ice sheet under crushing pressure. The experimental results of a 1:20 scaled CCG R-Class icebreaker model, and the full-scale turning circle results were used for validating the method.

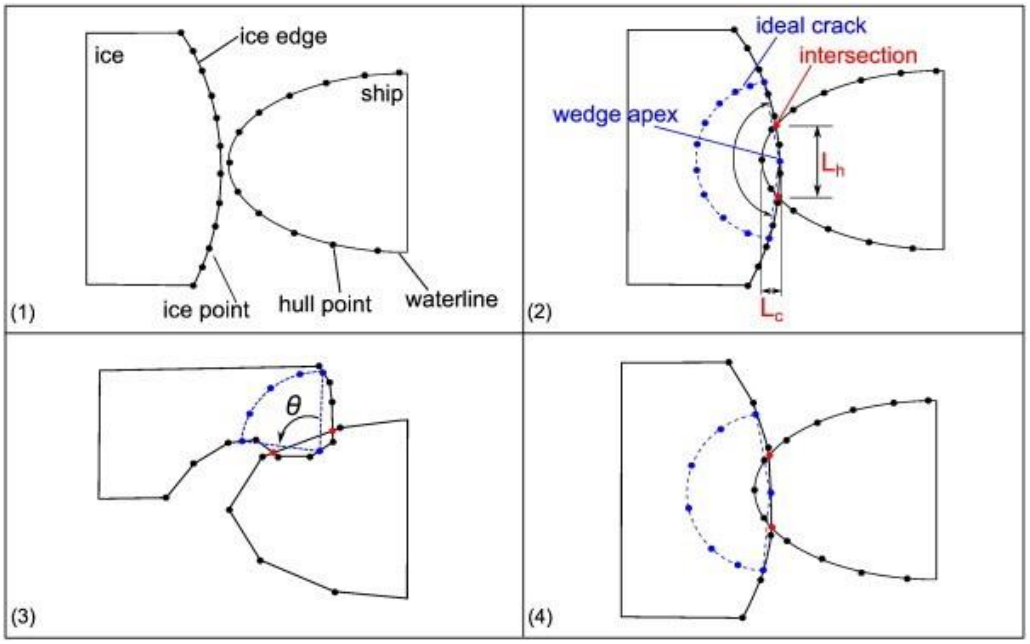

Fig. 2.3. Contact detection scenarios as illustrated in [13].

(1) no ice node is inside the ship and no ship node is inside the ice; (2) ice nodes are inside the ship and ship nodes are inside the ice; (3) ice nodes are inside the ship but no ship node is inside the ice; (4) no ice node is inside the ship but ship nodes are inside the ice.

2.3 Summary

A fully-numerical solution with appropriate modeling of both hydrodynamics and ice mechanics demands extensive modeling and computation resources. Because of this, many of the models studied in this section presuppose an idealized contact scenario, employ a combined numerical and semi-empirical solution, and assume a simple crack propagation process with no energy lost. Although simple, these choices provide a reasonable approximation of the ship-ice interaction. As GEM would benefit most from a reasonable, fast estimate of ice resistance, this work adopts a similar approach in Chapter 3.

Chapter 3: Model and Software Description

Estimating the resistance experienced by a ship operating in sea ice is a problem that includes many complex physical processes. Previous research on ice resistance simplified the physical interaction to provide a reasonable mathematical model of the ship-ice interaction. Examples of these simplifications include: assuming idealized contact geometry and symmetrical ice loads on different hull sections; using quasi-static formulas for irreversible processes; and the assumption that the total resistance can be broken up into multiple components which can be isolated and studied independently. This chapter describes the physics simulator architecture of GEM and derives a mathematical model of level ice breaking ice based on previous studies [8], [11], [13], [43], [45] which adopted much of the simplifications cited in Chapter 2.

3.1 Simulation Software Overview

3.1.1 Physics Kernel Overview

The user starts by loading the scene viewer, shown in Fig. 1.3, to simulate an ice scene in GEM. An ice scene could be created via the UI or loaded from a file. Additionally, the UI allows for the set up of ice floe parameters, ship properties, and the environmental conditions of the scene. The ice scene has one global coordinate system and a local coordinate system for each object. When the user starts the simulation for a chosen time span, GEM creates a simulation thread with a dedicated physics kernel. The architecture of the physics kernel is shown in Fig. 3.1. The initial conditions of the simulation are extracted from the graphical objects of the ice scene and converted into rigid body physics objects. The simulation then runs for a number of iterations determined by the time step and time duration set by the user. After all physics

updates have been computed in a given time step, a graphics frame is constructed and sent to the scene viewer thread so the user can view the simulation outcome in real-time.

To achieve hyper-real-time simulation performance, GEM has the option to run in multi-thread mode where each thread is responsible for a percentage of the ice floes in the scene. Furthermore, each thread constructs a list of neighbour references for every individual floe assigned to it, which can include neighbouring floes in adjacent threads. The neighbour list consists of any floes inside the region where the two polygons might collide soon. As a result, only the neighbours of a floe are considered for collision tests, rather than every object in the scene. The threads update the list of neighbours after syncing at the start of each physics update iteration.

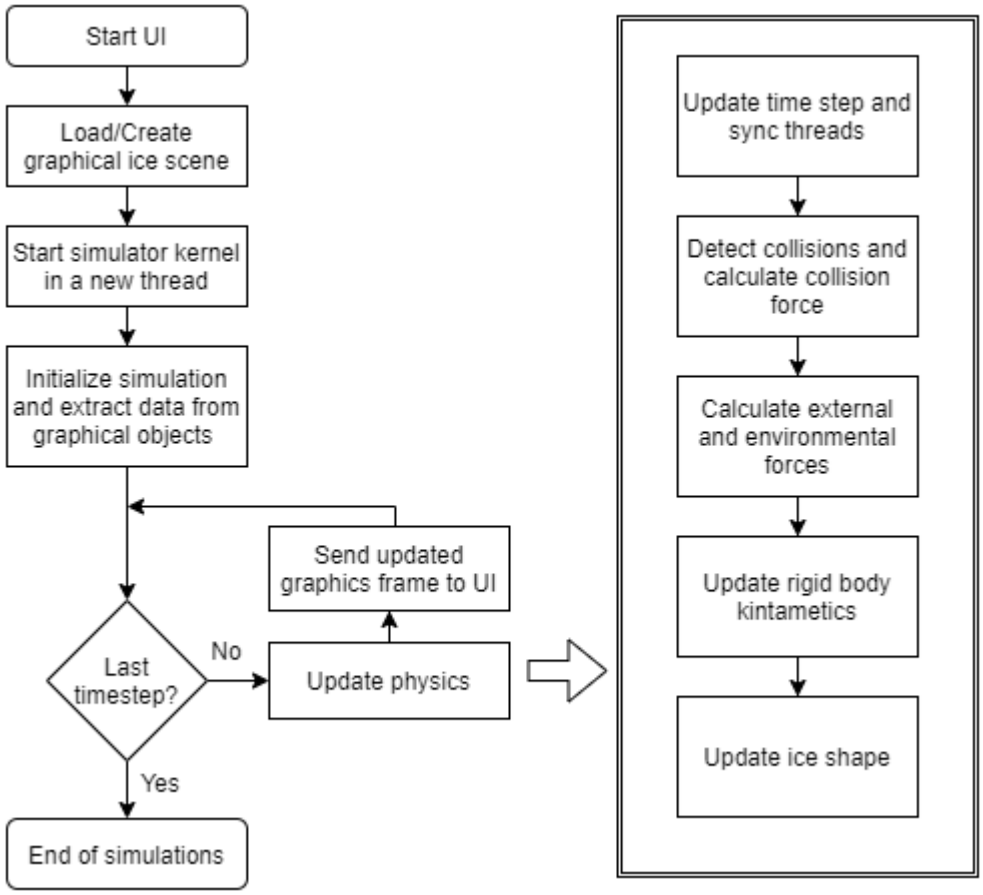

Fig. 3.1. The internal structure of GEM.

3.1.2 Collision Detection

After syncing all threads, collisions are identified by searching for possible overlaps between ice floes. As mentioned in [26], testing for collision between ice floes is comprised of two steps: determining whether the floes are overlapping, and computing the region of overlap formed by the intersection of the ice floe polygons.

To determine if two convex polygons are intersecting, the method of separating axes [49] is used. Separation of Axes provides a fast generic algorithm to test whether or not two convex objects are intersecting. It removes the need to have a collision detection code for every possible pair type (i.e., the vertex arrangement and number of edges the polygons have do not make a difference). The test for the overlap of two convex objects is stated as: "If there exists a line for which the intervals of projection (the lowest and highest values of the polygon projection on the line) of the two objects onto that line do not intersect, then the objects do not intersect". This line is known as the separating line or the separating axis.

For a pair of 2D convex polygons, only a limited set of direction vectors needs to be considered for separation tests which are the vectors normal to the sides of the polygons. The left illustration in Fig. 3.2 shows the case of two non-intersecting polygons separated along an axis defined by the normal to an edge of polygon C1. The right illustration shows two polygons that are not separated on any axis, and thus, they intersect. If an overlap is detected between two polygons, their intersection, convex hull, and contact point are computed using the intersection algorithm developed by Toussaint [50].

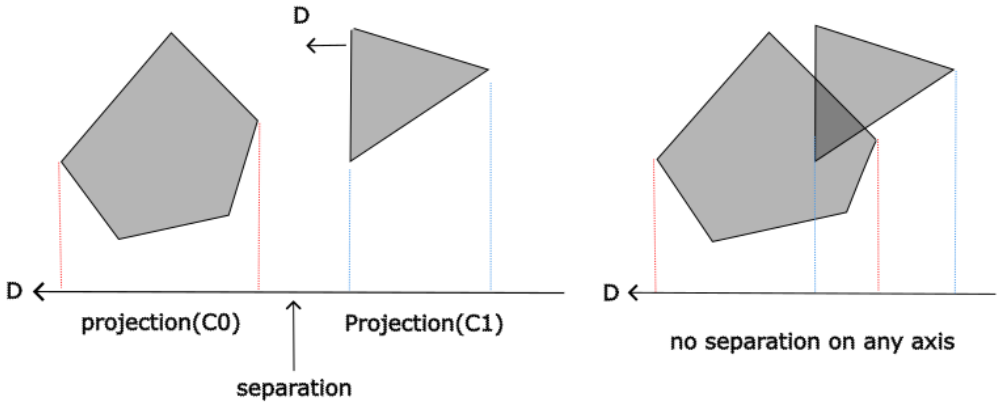

Fig. 3.2. Non-intersecting convex polygons (left) and intersecting convex polygons (right) as illustrated in [49].

The collision detection and polygon intersection algorithms can only be applied to convex polygons but ice floes can have a concave or convex shape due to natural processes or ice breaking. By partitioning concave polygons into several convex ones, contact detection and polygon intersection could be applied to each convex sub-polygon individually. The decomposition algorithm described by Fernández [51] is used to partition concave ice floes at the end of every iteration. An example of a compound concave polygon is shown in Fig. 3.4.

For concave ice floes, it is possible for a collision event to result in more than one overlap region between the two polygons. Therefore, GEM stores the overlaps for each of the convex sub-polygons in addition to the union between them, if it exists. The individual contact regions could then be utilized to calculate the collision forces generated by a ship-ice impact.

3.1.3 External Forces and Kinematics

In the step solving for rigid body kinematics, the total forces and moments for a physics object could be expressed mathematically as:

$$F_{total} = F_E + F_H + F_P + F_R \quad (23)$$

Where F_E is the environmental forces such as water, wind, and ice forces; F_H is the hydrodynamic force; F_P is the propeller force; and F_R is the rudder force. Each term consists of three force components in the local x, y, z directions of the physics object. As GEM models ice-ice impacts as well, some of the aforementioned forces could be zero, such as the rudder force (F_R) experienced by ice floes. The force due to environmental factors is described by:

$$F_E = F_{WT} + F_{WD} + F_{ice} \quad (24)$$

Where F_{WT} is the term for water-induced forces (e.g., water friction drag on ice floes); F_{WD} is the term for wind-induced forces (e.g., wind drag); and F_{ice} is the term for ice-induced forces. In each physics iteration, the acceleration of each object is deduced from the total force it experiences and the mass of the object. The change in velocity is then derived from the predicted acceleration based on the timestep.

3.1.4 Ice Shape Updating

GEM currently employs a simple form of ice breaking based on an edge-breaking model described by Daley et al. [52]. This model was developed to provide a better estimate of the force generated by an impact between a ship and an ice floe. Further, it was applied to study the safe operating speeds for ships in ice-infested waters. It was assumed that the ship only interacts with the ice in an impact event where the kinetic energy is fully consumed. The impacts always result in the maximum penetration possible based on Popov's energy equation [27]. The solution for the energy equation requires that the force is defined as a function of indentation. The effect of relative speed and the difference in mass is considered in solving for the collision force.

Broken ice floes are assumed to be circular in shape with a radius that is a function of ice thickness. GEM solves for the intersection of a circle (blue circle in Fig. 3.3) centred at the point of impact and the ice polygon. If an intersection exists, the two intersection points are saved, and the ice crushing force is compared to the bearing capacity of the ice floe. The forces are adjusted to account for the friction between the hull and the ice.

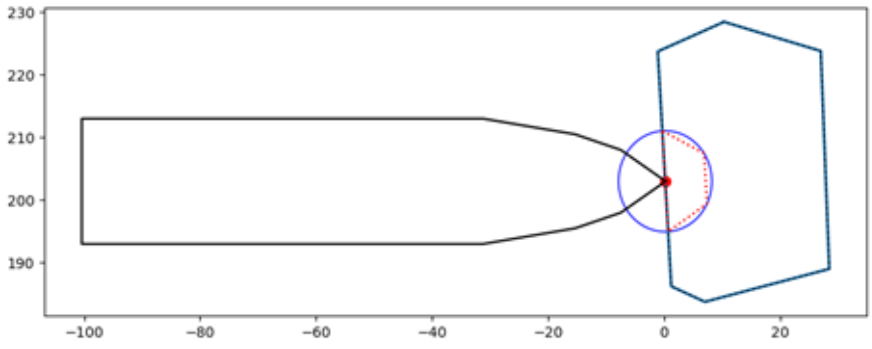

Fig. 3.3. The crack sequence (in red) generated from a ship-ice impact (unit: m).

If the vertical component of the crushing force exceeds the force needed to break the ice in flexure, a crack sequence is computed, as illustrated in Fig. 3.3. The generated crack sequence is utilized in the "Update ice shape" step, shown in Fig. 3.1, to partition the ice floe into a compound polygon representing the original floe and a convex polygon representing the broken ice piece. Fig. 3.4 demonstrates the result of the "Update ice shape" step. Each concave sub-polygon is plotted in a different colour, and the convex hull constituting the compound polygon is indicated with a dashed line.

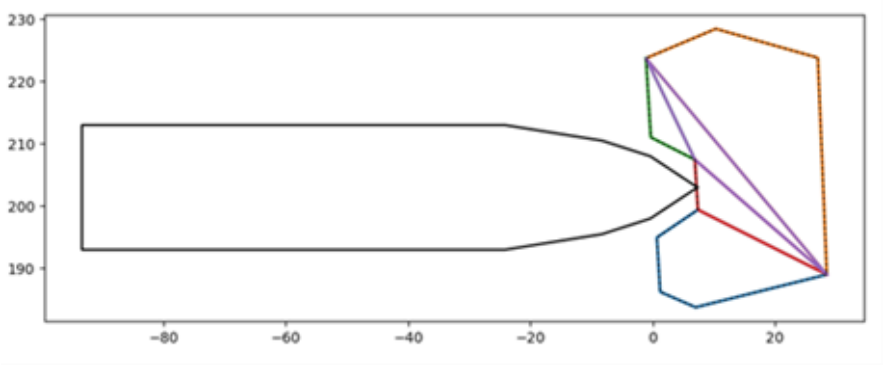

Fig. 3.4. The original compound ice floe after breaking (unit: m).

This approach is valuable for estimating the resistance and safe transit speeds in open pack ice, but it is incapable of simulating continuous level ice breaking. A core assumption is that the ice breaks once due to a ship-ice impact which consumes all kinetic energy and results in maximum penetration depth. As a consequence, it does not allow for repeated breaking events. Further, the ice resistance the ship experiences (F_{ice}) depends on the impulse caused by the impact, not the energy expended in breaking and clearing the ice. To account for the ice-induced forces (F_{ice}) experienced by a ship in a broken ice channel or advancing onto an ice plate; the following sections develop a new method for ice breaking.

3.2 Methodology

The same methodology of breaking the total ice resistance into separate components, presented in [3], [4], is applied in this thesis. The total ice-induced force is divided into three terms, i.e., crushing, breaking, and submergence, following Lindqvist's [8] model:

$$F_{ce} = F_{cr} + F_{br} + F_{sb} \qquad (25)$$

Where F_{cr} is the crushing force, F_{br} is the breaking force, and F_{sb} is the submergence force. Each term represents a vector comprised of three components: the surge force in the local x direction, the sway force in the local y direction, and the yaw moment around the local z axis.

The crushing force is incorporated into the breaking force as in [14], and thus Eq. (25) can be expanded as:

Where X_{ice} is the ice force component in the surge direction, Y_{ice} is the ice force component in

$$X_{ice} = X_{br} + X_{sb} \quad (26)$$

$$Y_{ice} = Y_{br} + Y_{sb} \quad (27)$$

$$Z_{ice} = Z_{br} + Z_{sb} \quad (28)$$

$$N_{ice} = N_{br} + N_{sb} \quad (29)$$

the sway direction, Z_{ice} is the ice force component in the heave direction, and N_{ice} is the yaw moment.

The following sections derive the terms for the ice crushing, breaking, and submergence forces.

3.2.1 Crushing Force

Ice crushing starts as soon as the ship contacts the ice. It continues from the initial time of contact until the vertical component of the generated crushing force is large enough to cause the ice to fail in flexure. As the broken ice edge is irregular, there could be more than one contact zone per simulation time step. The ice crushing force within each zone is normal to the contact surface in the direction of the hull. The ice crushing force F_{cr} per contact zone is given by:

$$F_{cr} = p_{ave} \,.\, A_{cr} \quad (30)$$

Where P_{ave} is the average pressure on the contact surface, and A_{cr} is the area of the crushing surface obtained from the contact detection algorithm.

Full-scale trials show that the contact pressure also varies with the contact area. This can be expressed by a widely accepted relationship known as the P-A curve [13]:

$$p_{ave} = p_0 \,.\, A_{cr}^{ex} \tag{31}$$

Where p_0 is the ice crushing strength, and ex is is a constant exponent. ex is typically a negative number, and it is assumed to be a tunable parameter in this thesis.

The contact scenario is assumed to result in an ideal ice wedge. Therefore, it can have two shapes, as illustrated in Fig. 3.5:

1- The penetration depth is less than ice thickness and the contact surface is triangular,
2- The penetration depth is greater than ice thickness and the contact surface is trapezoidal.

The area of the contact surface is then given by:

$$A_{cr} = \begin{cases} \frac{1}{2} L_h \frac{L_c}{\sin(\beta')} & L_c \le h_i . \tan(\beta') \\ \frac{1}{2} \left(L_h + L_h \frac{L_c - \frac{h_i}{\tan(\beta')}}{L_c} \right) \frac{h_i}{\cos(\beta')} & L_c \ge h_i . \tan(\beta') \end{cases} \tag{32}$$

Where L_h is the maximum width of the contact geometry, L_c is the maximum penetration depth, and β' is the normal frame angle of the hull at the contact point. L_h and L_c are numerically determined from the collision detection algorithm.

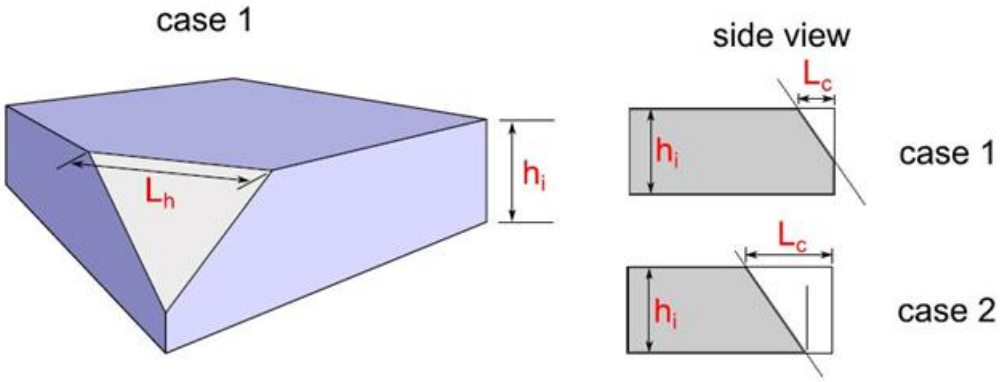

Fig. 3.5. Ideal ice wedge and contact surface as illustrated in [13].

The normal frame angle β' can be obtained from the frame angle β and waterline angle α as follows:

$$\beta' = \tan^{-1}(\tan(\beta)\cos(\alpha)) \tag{33}$$

Where the frame angle β is given by:

$$\beta = \tan^{-1}\left(\frac{\tan(\alpha)}{\tan(\gamma)}\right) \tag{34}$$

The frame angles along the hull of the ship can also be entered manually through the scene viewer. Further, GEM is able to calculate the missing hull angles from the ship polygon, given that enough data is available about the hull geometry.

3.2.2 Frictional Force

Ice crushing results in ice sliding along the hull, which generates a frictional force. Su et al. [11] proposed a method to calculate the frictional forces which is based on the relative velocity between the ship and ice plate. They also stated that the crushing force should be decomposed

into a horizontal and a vertical component to account for the two components of friction in the horizontal and vertical planes. The components of the frictional force are shown in Fig. 3.6.

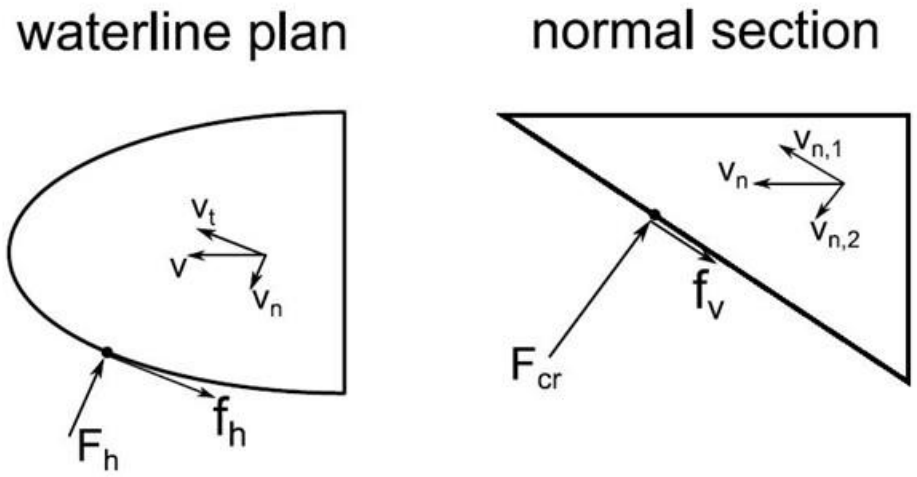

Fig. 3.6: Directions of force and velocity components as illustrated in [36].

The friction contribution to each component of the crushing force can be accounted for as follows:

$$f_h = \mu F_{cr} \frac{v_\tau}{\sqrt{v_\tau^2 + v_{n,1}^2}} \tag{35}$$

$$f_v = \mu F_{cr} \frac{v_{n,1}}{\sqrt{v_\tau^2 + v_{n,1}^2}} \tag{36}$$

Where v_τ is the tangential of relative velocity in the horizontal plane, $v_{n,1}$ is the normal velocity component tangential to the contact surface, f_h is the horizontal force component, and f_v is the vertical force component. The force directions and velocity components are shown in Fig. 3.6.

3.2.3 Breaking Force

To find the total ice breaking force, the crushing force adjusted to account for friction needs to be projected onto the local coordinate system of the ship. Based on the analysis in [13], the projections of the force components are given by:

$$X_{br} = \left(\sin(\beta')\tan(\alpha) + \mu\sqrt{1+\tan^2(\alpha)\cos^2(\beta')}\right).F_{cr} \quad (37)$$

$$Y_{br} = \left(\sin(\beta') - \mu\tan(\alpha)\frac{\cos(\alpha)-\cos^2(\beta')}{\sqrt{\cos^2(\alpha)+\sin^2(\alpha)\cos^2(\beta')}}\right).F_{cr} \quad (38)$$

$$Z_{br} = \left(\cos(\beta') - \mu\frac{\sin(\alpha)\sin(\beta')\cos(\beta')}{\sqrt{\cos^2(\alpha)+\sin^2(\alpha)\cos^2(\beta')}}\right).F_{cr} \quad (39)$$

X_{br} and Y_{br} are the ice breaking force components in the horizontal plane and Z_{br} is the vertical component of the ice breaking force. Z_{br} is the force acting down on the ice plate and can be further compared to the bearing capacity of ice to determine whether flexure failure occurs at a given time step.

The breaking yaw moment can then be obtained by:

$$N_{br} = -X_{br}.y + Y_{br}.x \quad (40)$$

Where x and y are coordinates of the contact point in the local ship frame.

The total ice breaking force on the ship is attained by integrating all projected crushing forces for each contact zone along the entire hull of the ship.

3.2.4 Breaking Due to Bending

The vertical component of the ice breaking force increases as the ship advances onto the ice sheet. Bending failure occurs when the vertical force exceeds the bearing capacity of the ice and a circular ice floe breaks off the ice plate. A formula to calculate the bearing capacity of an ice plate was presented by Kashtelyan [53] as:

$$P_{flex} = C_f \left(\frac{\theta}{\pi}\right)^2 \sigma_f \, h_i^2 \qquad (41)$$

Where C_f is an empirical coefficient; θ is the angle of the ideal ice wedge, illustrated in the third scenario in Fig. 2.3; and σ_f is the flexural strength of the ice plate. The formula represents the bearing capacity for quasi-static loading. As a consequence, it is only suitable for low-velocity interactions. The model developed in this thesis is intended to be simple and only provide an engineering estimate of the forces involved by sacrificing some accuracy. Thus, the ice plate dynamics are beyond the scope of this work, and Kashtelyan's formula is assumed to suit all speed profiles.

Kashtelyan [53] suggested a value around 1.0 for C_f. Nguyen et al. [38] considered C_f to be 4.5. Su et al. [11] studied the effects of bearing capacity and determined the empirical coefficient to be equal to 3.1. Zhou et al. [13] adopted a value of 2.2 after conducting a study to determine the appropriate values for the coefficients in semi-empirical ice resistance formulas. The model proposed in this thesis considers C_f to be a tunable parameter. However, the experiments conducted in this study use the value presented in the findings of Zhou et al.

3.2.5 Correcting for Ice Flexural Deflection

Early works on numerical ice breaking [11], [38], [43] assumed a rigid ice plate model that did not consider the vertical deflection caused by the bending of the ice plate. Zhou et al. [13] proposed a simple method to correct for the flexural deflection of the ice based on the work of Valanto [16], where water is considered as an elastic foundation. Further, it is assumed that the deflection of the ice plate is minuscule compared to the characteristic length of ice. Subsequently, it could be seen as a parallel downward movement of the ice plate instead of bending.

As shown in Fig. 3.7, from the initial contact instant, the ship penetrates into the ice by δ_s which results in a downward elastic deflection of the plate by δ_e and a vertical crushing height of δ_c. $\delta_s, \delta_e, and\ \delta_c$ satisfy the following expression:

$$\delta_e + \delta_c = \frac{\delta_s}{\tan(\beta')} \tag{42}$$

Where δ_e, δ_c are caused by the vertical component of the ice crushing force, F_{cr}.

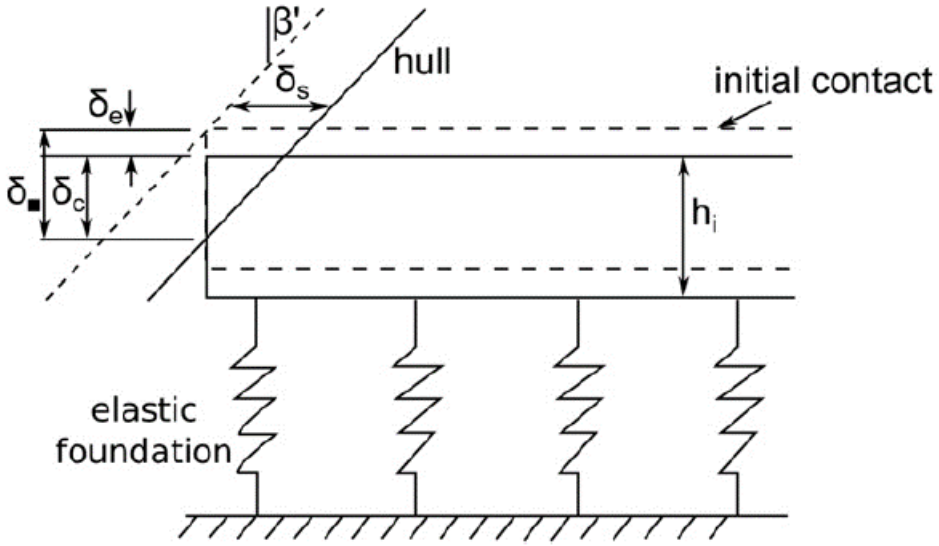

Fig. 3.7. Flexural deflection of ice plate as illustrated in [13].

Zhou et al. [13] derived the relation between δ_e and F_{cr} by considering the response of a homogeneous and isotropic elastic ice plate with a wedge angle equal to θ. The plate was assumed to be resting on a fluid foundation with a static vertical concentrated load on the wedge apex. Kashtelyan [53] presented the following expression to calculate the deflection at the apex of a semi-infinite plate:

$$w_0 = \frac{1}{2}\left(\frac{\pi}{\theta}\right)^2 \frac{P}{\sqrt{\gamma D}} \qquad (43)$$

Where P is the vertical load, γ is the weight per unit volume of the liquid, and D is the flexural rigidity of the ice plate.

γ and D are given by:

$$\gamma = \rho_w g \qquad (44)$$

$$D = \frac{E.h_i^3}{12\,(1-\nu^2)} \tag{45}$$

Substituting P, w_0 with $F_{cr,v}, \delta_e$ in Eq. (43), the following relationship was derived:

$$F_{cr,v} = \frac{2\,\theta^2}{\pi^2}\sqrt{\rho_w \,.\, g \,.\, D}\,.\,\delta_e \tag{46}$$

δ_c is obtained through an iterative numerical solution.

The crushing force can then be adjusted by modifying A_{cr} in Eq. (30) to account for the reduction in contact area due to the flexural deflection of the ice plate. The revised crushing force is expressed as:

$$F_{cr}^{*} = p_{ave}\,A_{cr}\left(\frac{\delta_c}{\delta_v}\right)^2 \tag{47}$$

The flexural deflection of the ice sheet can then be corrected for by replacing F_{cr} with F_{cr}^{*} in Eqs. (37), (38), and (39).

3.2.6 Broken Ice

If Z_{br} is greater than P_{flex}, flexural failure occurs, and an ice piece breaks off the ice plate. Otherwise, the ice is only crushed. The size of the ice piece depends primarily on the characteristic length of the ice, l_c, given by Eq. (12), and the relative velocity component perpendicular to the contact surface. The radius of the broken floe is expressed by Wang [43] as:

$$R = C_l . l_c . (1 + C_v v_{n,2}) \quad (48)$$

Where R is the radius of the circumferential crack, C_l is a coefficient that defines the size of the broken ice relative to the characteristic length of the ice plate, C_v is an empirical coefficient considered to be tunable in this thesis, and $v_{n,2}$ is the relative velocity component normal to the contact surface.

3.2.7 Submergence Force

Zhou et al. [13] derived a model to solve for the y-component of ice buoyancy based on [45]. They assumed that the hull is port-starboard symmetric, and the ice forces act on the bow and midship part of the ship. They further considered that the directions of buoyancy and clearing forces should be the same as that of the breaking force. In the model of Zhou et al., the clearing and buoyancy terms from [14] were used. For the surge component of submergence force, they proposed utilizing the following equations for buoyancy and clearing force by Spencer & Jones [14]:

$$X_{cl} = 2.03\, F_h^{-0.971} \rho_i B h_i v_{surge}^2 \quad (49)$$

$$X_{bu} = 2.67 \Delta \rho g h_i B T \quad (50)$$

However, as this thesis is also concerned with ice management, the submergence term in [8] was also investigated. The submergence term from Lindqvist is provided as:

$$R_S = \rho_\Delta . g . h_i . B \left(\frac{T(B+T)}{B+2T} + \mu \left(A_u + \cos(\bar{\gamma}) \cos(\bar{\psi}) A_f \right) \right) \quad (51)$$

In Eq. (13), the ice resistance due to submergence was derived based on the difference in density, ρ_Δ; the area of the flat bottom, A_u; and the bow area, A_f. This equation enables a wider variety of ice management scenarios as the breaking resistance can be calculated independently based on the area of the broken ice in contact with the ship. The model derived in this section maintains that a maximum of 70% of the length of the ship could be covered in broken ice with L and B approximated from the geometry of the overlaps between the hull of the ship and the broken ice. However, it should be noted that a more reliable estimate can be reached by deriving the expressions for A_u and A_f in Eq. (51) for the hull form in question.

Consequently, the y-component of submergence resistance is given by:

$$Y_{sb,bow} = \frac{X_{sb}}{2} \cdot \frac{Y_{br}}{X_{br}} \quad (52)$$

Where X_{sb} is the x-component of the ice resistance due to submergence given by Eqs. (7) and (13); and X_{br}, Y_{br} are the horizontal components of the ice breaking force from Eqs. (37) and s(38), respectively.

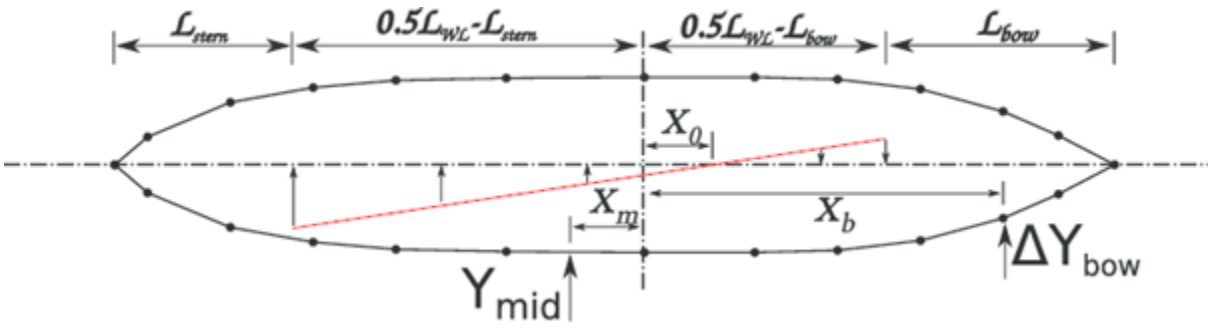

Fig. 3.8. Arms of rotation as illustrated in [13]

If the ship is moving straight in the surge direction, the ice load should be equal on both sides of the hull. However, the load ceases to be symmetrical as the ship starts turning in ice.

According to [13], the load on the bow due to turning can be expressed as:

$$\Delta Y_{sb,bow} = v_{surge} \frac{\sin(\theta_1)}{\tan(\alpha)} . Y_{sb,bow} \quad (53)$$

Where θ_1 is given by:

$$\theta_1 = atan2\left(r.\frac{L_{WL} - L_{bow}}{2}, v_{surge}\right) \quad (54)$$

Where r is the angular velocity around the z-axis, v_{surge} is the surge velocity of the ship, L_{WL} is the ship length at the design waterline, and L_{bow} is the length of the bow as illustrated in Fig. 3.8.

The ice load on the parallel midship section is considered to be in the direction opposite to sway velocity and is given by:

$$Y_{sb,mid} = C_{mid}\, X_{sb} \frac{v_{sway}}{v_{surge}} \quad (55)$$

Where v_{sway} is the sway velocity; and C_{mid} is an empirical coefficient provided as 2.0 in [13] and considered to be tunable in this thesis.

The yaw moment due to submergence force can then be obtained through:

$$N_{sb} = \Delta Y_{sb,bow} . x_b + Y_{sb,mid} . x_m \quad (56)$$

Where x_b, x_m are the lever arms illustrated in Fig. 3.8 and can be attained from the following expressions:

$$x_m = \frac{\frac{1}{3}L_1^2(L_1 r + v_{sway}) - \frac{1}{3}L_2^2(L_2 r + v_{sway})}{0.5L_1(L_1 r + v_{sway}) + 0.5L_2(L_2 r + v_{sway})} \quad (57)$$

$$x_b = \frac{1}{2}L_{WL} - \frac{1}{2}L_{bow} \quad (58)$$

Where:

$$L_1 = \frac{1}{2}L_{WL} - L_{stern} + x_0 \quad (59)$$

$$L_2 = \frac{1}{2}L_{WL} - L_{bow} - x_0 \quad (60)$$

Where L_{stern} is the length of the stern, L_{bow} is the length of the bow, and x_0 is described as:

$$x_0 = -\frac{v_{sway}}{r} \quad (61)$$

3.3 Summary

This chapter describes the current structure of GEM and derives a ship-ice interaction model that is compatible with its internal architecture. The model simulates the physical interaction process through a combined numerical and semi-empirical solution. Running the model in the time domain produces a time history of the ice forces a vessel experiences as it advances into level ice. The next chapter describes the details of integrating the proposed model into GEM, the relevancy of the model for ice management, and presents the results from several validation experiments based on model-scale and full-scale test data.

Chapter 4: Model Implementation

This chapter describes the integration of the proposed model into GEM. The simulation program feature is implemented with the programming language C++ using the Qt graphical application development framework.

4.1 Numerical Model Overview

The ice breaking model implementation, shown in Fig. 4.1, is meant to be integrated as an additional feature into the existing open pack ice simulation, described in section 3.1. The collision detection changes starting from “Collision detection entry point” are described in section 4.2, Ice force calculations and crack generation are described in section 4.4, and ice shape updating is detailed in section 4.5.

Any simulation run can be designated as a level ice breaking simulation using an input flag. When designated as a level ice simulation, the execution flow of the software branches from the open pack ice design at two distinct points: The “Detect Collision and Calculate Collision Force” step and the “Update Ice Shape” step, shown in Fig. 3.1. This design choice allows for a seamless transition between the two categories without breaking any existing features in GEM. The same ice scene can be simulated with the level ice flag set or cleared without having to reset or recompile the program. Frames from the output of a simulation run under any of the two categories can be saved as an ice scene and run under a different interaction model configuration. Moreover, this design decision would set the ground for future development aiming to combine both models.

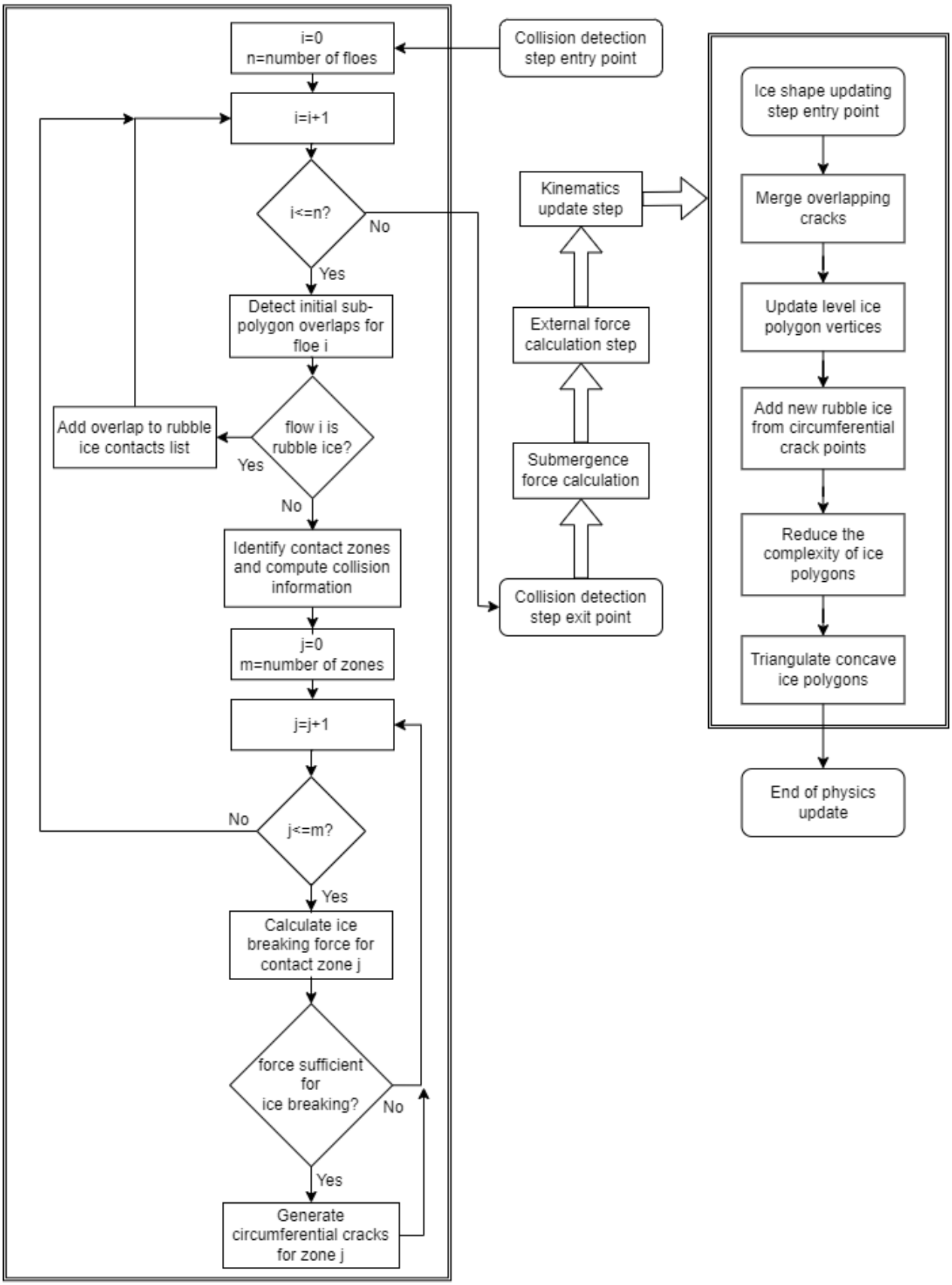

Fig. 4.1. GEM ice breaking model flow.

4.2 Collision Detection

First, overlaps are computed according to the Collision Detection step described in section 3.1.2. The output of that step, illustrated in Fig. 4.2, contains the overlap information between the convex sub-polygons of any two intersecting objects. In this study, only the intersections between vessels and ice objects are considered for level ice simulations. Further, only a single ship is assumed to be traversing a level ice sheet at a given time step.

In the original implementation, collision information would be evaluated separately for each sub-overlap. This approach is feasible as the collision force in open pack simulations is calculated per floe, not per collision. However, when traversing level ice, multiple unique zones of ice crushing could exist simultaneously. Thus, it is essential to be able to identify the extent of each continuous zone where the crushing of the ice edge is occurring. Overlaps between the ship and broken ice floes are considered separately.

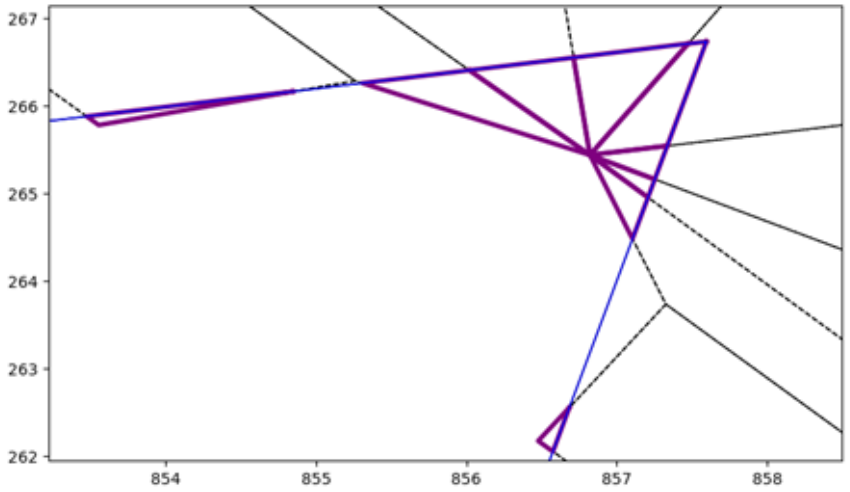

Fig. 4.2. Sub-polygon overlaps (purple) between the hull of the ship (blue) and the ice plate (black) (unit: m).

4.3 Identifying Contact Zones

The level ice breaking algorithm identifies adjacent overlaps through shared edges and marks them as “neighbours”. Neighbouring overlaps are merged into a contact zone, as shown in Fig. 4.3. The contact zones in this study follow the contact zone description in [13]. The geometry of a zone is considered to be the convex hull of adjacent sub-polygon overlaps, obtained by the Graham scan method [54]. The overlap information is then re-evaluated for the merged area.

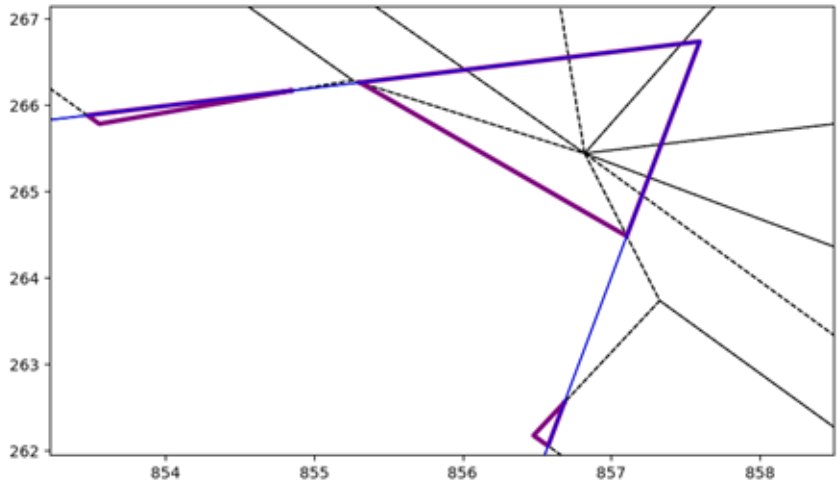

Fig. 4.3. Contact zones (purple) between the hull of the ship (blue) and ice (black) (unit: m).

As concluded by [55], there is no “correct” shape for a set of points in a plane. Therefore, all concave hull algorithms must rely on tunable parameters to be able to terminate. Changing the value of these parameters for the same set of input points generates varied shapes belonging to the same “family”. Consequently, any comparison of the shapes produced by different algorithms must account for these differences. Further, there is no standard experimental design that considers parameterization differences when assessing the viability of different concave hull algorithms for a specific application. Thus, the use of a concave hull algorithm is deemed out of scope, and a convex hull representation is considered an acceptable approximation. The convex hull of the overlap geometry is utilized as it simplifies the force calculations.

Furthermore, the Graham scan algorithm [54] has an average time complexity of $O(n \log n)$. In contrast, the uncommon best case for most concave hull algorithms, such as alpha shapes, has a time complexity of $O(n \log n)$, excluding the postprocessing needed to validate the output [55].

4.4 Ice Force Calculation

The contact surface area per zone is calculated using Eq. (32). L_h and L_c are determined numerically through the geometry of the contact zone. The average pressure is then obtained through Eq. (31). Ice crushing force and the resulting frictional forces are obtained using Eqs. (30), (35(35), and (36). The change in the contact area due to flexural deflection is detected by numerically solving for the delta parameters in Eq. (47). The components of the ice breaking force and yaw moment are derived from the adjusted ice crushing force using Eqs. (37), (38), (39), and (40). Lastly, the bearing capacity of the ice plate is obtained through Eq. (41) and compared to the vertical component of the ice breaking force from Eq. (39).

4.4.1 Circumferential Crack Generation

If the vertical component of the ice breaking term is larger than the bearing capacity of the ice plate, the ice fails in flexure and a circumferential crack is created. The crack sequence is generated as described in section 3.1.4. However, as shown in Fig. 4.2, multiple contact zones per time-step can be present during level ice breaking. Therefore, the crack generation method is applied to each current contact zone. Eq. (48) is used to determine the radius of the intersection test representing the circumferential crack width based on the findings of Wang [43]. The sequence generated by each failure event is saved to a list and later utilized by the "Ice shape updating" step to break off rubble ice polygons.

4.4.2 Ice Submergence Force

The solution for submergence force is decoupled from the ice breaking force calculation step. If Lindqvist's solution is utilized, the vertices of all submerged ice overlaps are aggregated for later processing in the collision detection step. The total contact area between submerged ice and the hull is derived from the convex hull of all submerged ice overlaps. This approach allows for versatile ice management simulations as ships traversing a broken ice channel still experience ice resistance from submerged pieces. When using Lindqvist's solution, only floes marked as "rubble ice" contribute to the ice submergence force. Rubble ice floes are generated by ice breaking events or marked as such in the initial ice. Floes cannot be manually marked as rubble ice when a simulation is in progress. The ice-covered areas of Eq. (51) are derived from the total submerged ice contact area. The ice submergence force and yaw moment are then calculated using Eqs. (53), (55), and (56). However, the rest of this study follows another available option: the buoyancy and clearing force solution proposed by Zhou et al. in [13], given by Eqs. (49) and (50), as calculating the submergence force per ice floe is computationally expensive, making GEM simulations impossible to run in real-time.

4.5 Ice Shape Updating

The ice shape updating for level ice sheets utilizes the circumferential crack sequences generated by the collision detection step to update the vertices of the sheet ice polygon and generate the broken ice floes. If the crack sequence point is valid, new vertices are added to the sheet ice polygon. Old ice edge vertices that are a part of the breakoff piece are removed from the ice polygon and reassigned to the break off floe.

4.5.1 Polygon Tessellation

As mentioned in section 3.1.2, GEM can only test for collisions between convex shapes. Therefore, concave polygons have to be decomposed into convex sub-polygons to enable collision detection in a process known as tessellation. Convex partitioning (tessellation) satisfies the requirements for open pack ice simulations. However, the increase in vertex density and the sharper angles resulting from continuous ice breaking often cause faults in convex partitioning. Moreover, most convex partitioning algorithms, such as Keil-Snoeyink [56] and Hertel-Mehlhorn [57], start with a tessellation of the polygon into triangles and then merge the triangles to construct the convex sub-polygons. Thus, for the case of ice breaking in GEM, it is more efficient to tesselate the ice polygons into triangles, also called polygon triangulation.

In this study, ice polygons are partitioned according to the "triangulation" step of the dynamic-programming algorithm of Keil and Snoeyink [56]. The resultant triangles are optimal in terms of minimal edge length. The goal of the algorithm is the tessellation of a polygon P, with edges sorted in counter-clockwise order, into a canonical triangulation. It assumes that each convex region C has at least one vertex that was reflex in P. A reflex is a vertex where the interior angle between the polygon edges that connect at the vertex is greater than $180°$. The reflex with the lowest index in C is connected to all vertices with a higher index in C. If the tessellation of C is not yet achieved, the vertex with the highest index is assumed to be a reflex in P. It is then connected to the remaining vertices in that convex region. Fig. 4.4 shows an example from [56] in which "vertices between p_8 and p_{12} and between p_{20} and p_{26} connect to the highest index in their region; all other vertices connect to the lowest". Fig. 4.5 shows the output of the algorithm when applied to an ice edge in GEM.

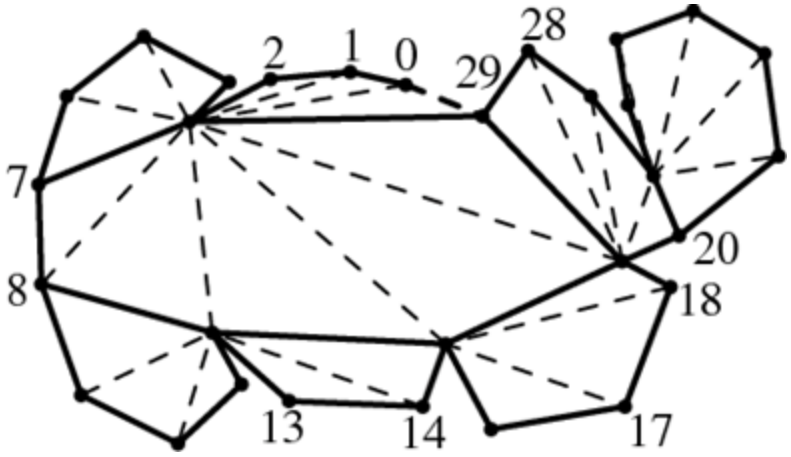

Fig. 4.4. Canonical triangulation from minimum decomposition as illustrated by [56].

The algorithm has a time complexity of $O(n^3)$. Although faster algorithms are available, such as the Monotone Partitioning method described in [58] with a time complexity of $O(n\ log\ n)$, they tend to produce thin triangles when the density of vertex distribution along the ice edge is high. Thin triangles cause glitches during collision detection in GEM as the impact of rounding errors becomes significant.

4.5.2 Polygon Noise Reduction

With each ice breaking event, new vertices are added to the sheet ice polygon to define the current shape of the ice edge. Considering that the tessellation algorithm uses existing vertices as anchors to triangulate the compound polygon, new sub-polygons have to be created to describe the ice shape. Consequently, the number of computations per frame increases significantly as collision detection is done per convex sub-polygon. For example, the polygon in Fig. 4.5 has 349 vertices and generated 347 triangles after partitioning. Most of these vertices are at the ice edge and add complexity without contributing to simulation accuracy. Furthermore, the features defined by these vertices persist even if they are unlikely to be a part of an interaction. Thus, reducing the number of redundant features is crucial for preserving the hyper-real-time performance of GEM.

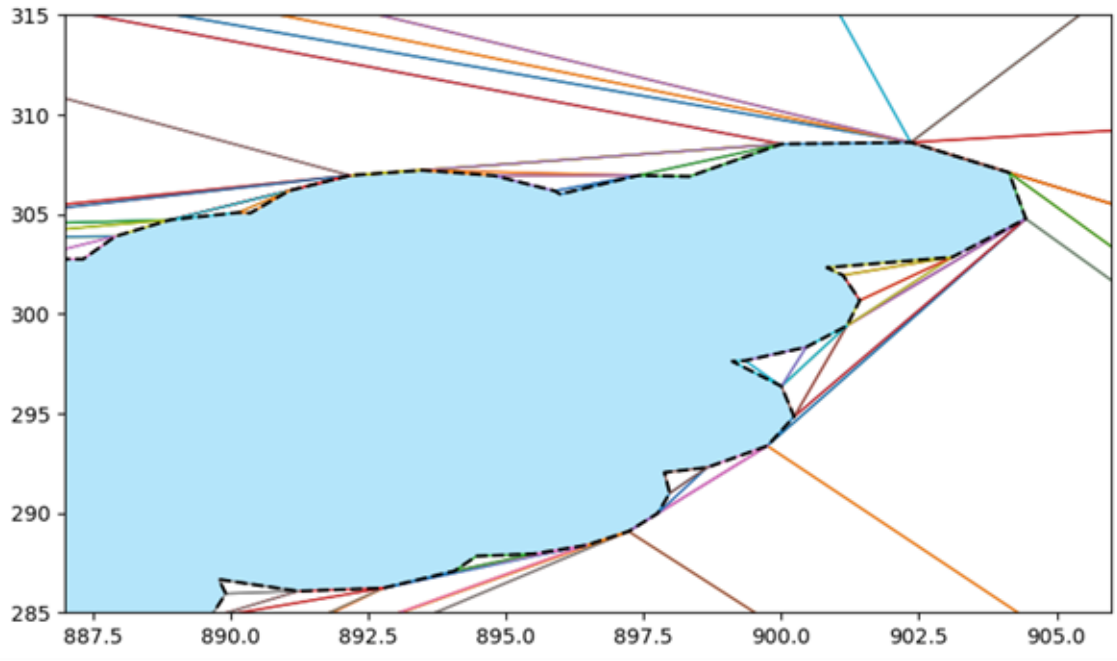

Fig. 4.5. Convex sub-polygons (colored triangular polygons) generated from the tessellation of the ice plate (black dashed outline) at the ice-water edge (unit: m).

The Ramer-Douglas-Peucker algorithm [59], [60] is a curve simplification algorithm first developed for cartographic generalization. Cartographic generalization is concerned with deriving smaller-scale maps from high-level-of-detail map data. For example, the outlines of buildings in a city block are reduced to a general outline of that block. The goal of the algorithm is, given a collection of line segments constituting a curve, also called a polyline, to find a similar polyline with fewer points. In this study, the input polyline is the outer ring of an ice polygon, excluding the edge connecting the first and last vertices. The similarity between the two polylines is based on the maximum distance between the original curve and the desired simplified one. The resultant simplified polygon consists of a subset of the vertices that defined the outer ring of the original polygon. Ramer-Douglas-Peucker has an average time complexity of $O(n \log n)$ and a worst-case of $O(n^2)$ [61].

A distance tolerance, epsilon, is used to determine termination. The higher the tolerance, the less noisy the output is. Epsilon is considered a tunable parameter in this study. The effect of

different values of epsilon on ice edge vertices is illustrated in Fig. 4.6. The algorithm starts with the assumption that there is a single edge joining the first and last vertices of the original polygon, which are referred to as the anchor point and the floating point, respectively. It then calculates the perpendicular distance between all remaining vertices and that edge. The furthest vertex from the start edge, which has a perpendicular distance greater than epsilon, is marked as a key and added to the simplified polygon. This process is done recursively for each edge in the current simplification. The algorithm terminates when the original and simplified polygons are within tolerance and no new keys can be found.

Fig. 4.6. Simplified ice edge for different values of epsilon.

The Ramer-Douglas-Peucker algorithm is utilized in two distinct ways in this study. In the original implementation [60], an arbitrary number of points is removed based on the distance tolerance parameter. However, the algorithm could also be modified to limit the number of vertices per polygon to a specific value, N. To realize this, the possible edges of the simplified polygon are computed recursively and sorted in descending order based on their point-edge distance. The vertices of the simplified polygon are considered to be the keys to the first N edges in the sorted list. This algorithm variant is utilized to keep the number of vertices per polygon (N) under the maximum allowed by GEM at the expense of accuracy. The value of N is thus dependent on hardware constraints.

4.6 Summary

This chapter discusses the implementation of the proposed model as a feature in GEM. The ice-induced forces are obtained using the methodology in Chapter 3. After each failure event, the ice edge is updated based on generated circumferential cracks. The updated ice shape is simplified by removing redundant vertices to reduce the number of computations per time step. Lastly, ice polygons are triangulated to facilitate collision detection with the complex concave shapes created by ice breaking.

Chapter 5: Model Validation and Results

Multiple simulations were conducted based on model-scale and full-scale data to validate the numerical method presented in this thesis. The output of the validation simulations is then compared to published results. Two different vessels were selected for the validation simulations in this chapter: the Canadian Coast Guard icebreaker, Terry Fox, and the R-Class icebreaker, Sir John Franklin. The benchmark data includes the model-scale straight resistance runs of CCGS Terry Fox [45], and the full-scale sea trials of the R-Class icebreaker CCGS Sir John Franklin [14], [20]. In addition, the effect of polygon simplification on ice resistance was investigated. A range of distance tolerances are simulated, and the results are contrasted. The simulations were ran on an AMD Ryzen 9 5900HS CPU with 16.0 GB of RAM. Due to computational constraints resulting from the simulations being sequential and CPU-bound, the broken ice floes were not visualized nor considered for further processing in this chapter. Therefore, their contribution to ice resistance was only considered for the icebreaking vessel and would not apply to other vessels passing through the ice channel.

5.1 Effect of Simplification Distance Tolerance

To study the effect of simplification distance tolerance (epsilon), described in section 4.5.2, the Terry Fox model-scale tests, detailed in section 5.2, were conducted for multiple values of epsilon. Fig. 5.1 and Fig. 5.2 show a sample of the change in mean resistance and processing time, respectively, for the tests conducted at a surge velocity of 0.3m/s. Fig. 5.1 shows that the mean resistance increases with the increase in distance tolerance. The increase in resistance is due to polygon simplification removing some of the minor features which cause the cusps to break under less force. For example, sharp ice features are smoothed out, resulting in broader

wedge angles. As a result, the average contact area per collision is larger and more force is required to break a new cusp. In Fig. 5.2, it can be noticed that the processing time drops semi-exponentially with the increase in epsilon value. That is due to the reduced density of polygon vertices on the ice edge, resulting in fewer sub-polygons being generated and, consequently, fewer computations required for collision detection and force calculations. The tuning epsilon is more effective for smaller ships, test models, and sharp turns in ice as these are cases where smaller cusps are broken more frequently. Meanwhile, large vessels moving in a mostly straight path tend to break large uniform cusps and result in a lower density of polygon vertex distribution along the ice edge. A fixed distance tolerance value of 0.02 is chosen for the rest of the experiments in this study as it provides the most agreement with Terry Fox tests.

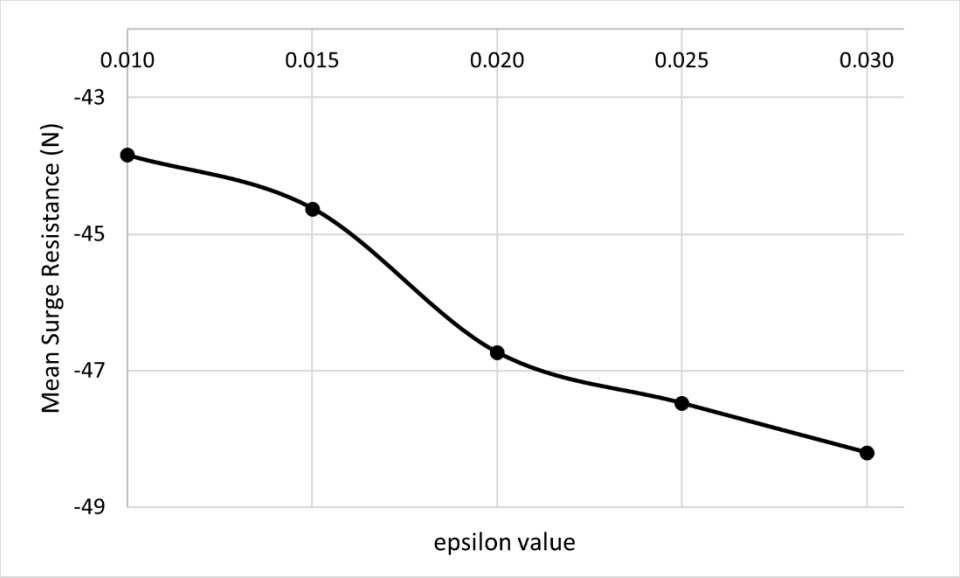

Fig. 5.1. Mean surge resistance against distance tolerance.

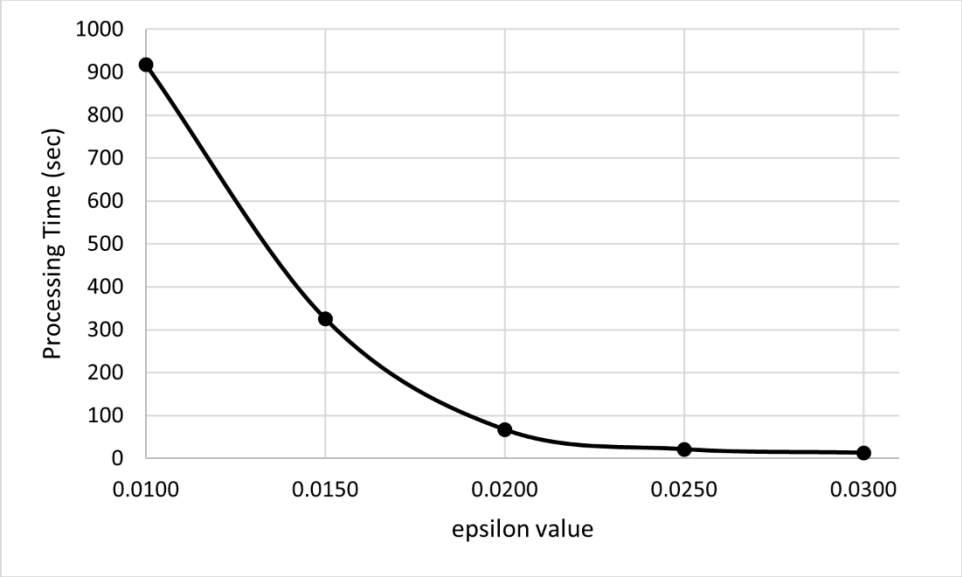

Fig. 5.2 Processing time against distance tolerance.

5.2 Terry Fox Model-Scale Tests

As described in [20], [45], The Institute for Ocean Technology (IOT) Terry Fox model is a 1:21.8 scaled model of the Canadian icebreaker, CCGS Terry Fox. The waterline of the model is shown in Fig. 5.3, and the Principal dimensions are presented in Table 5.1.

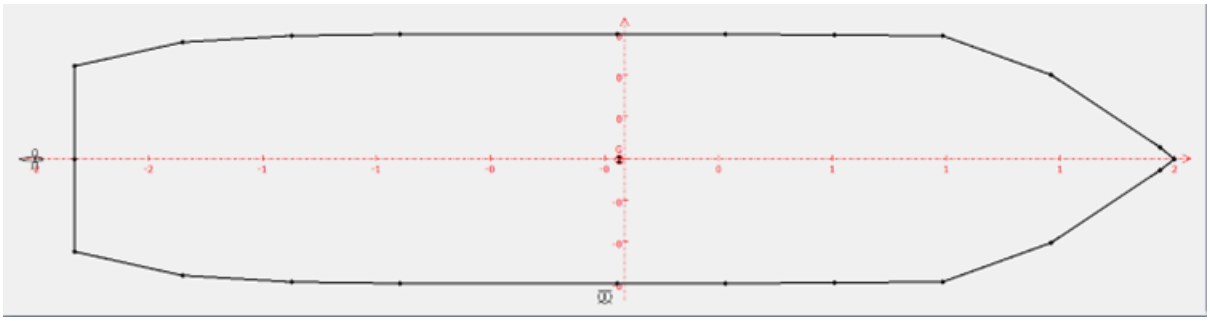

Fig. 5.3. Model-scale Terry Fox waterline profile (unit: m).

Table 5.1. Principal dimensions of the model-scale Terry Fox adapted from [45].

Parameter	Notation	Value	Unit

Length	L	3.485	m
Breadth	B	0.792	m
Draft	T	0.368	m
Mass	M	625.8	kg
Block Coefficient	CB	0.577	-

The results of Terry Fox model-scale tests have been published in [62] and [63]. The ice had a flexural strength of 35 kPa and a thickness of 40 mm. The simulation scene was created based on the same ice conditions, which are described in Table 5.2. The ice resistances are compared to test data. Fig. 5.4 presents a section of the time history of simulated ice resistance for IOT Terry Fox at 0.3m/s. Fig. 5.5 contrasts the mean resistance at different surge speeds between the simulation output and the test results published in [62] and [63].

Table 5.2. Ice mechanical properties for model-scale Terry Fox simulations adapted from [45]

Parameter	Notation	Value	Unit
Flexural strength	σ_f	35	kPa
Crushing strength	p_0	70	kPa
Ice thickness	h_i	0.04	m
Young's modulus	E	24.5	MPa
Poisson ratio	ν	0.33	N/A
Friction coefficient	μ	0.06	N/A
Ice density	ρ_i	910	kg/m^3
Simplification Distance Tolerance	ϵ	0.02	-

	C_f	2.2 [13]	-
	C_v	-0.5 [13]	-

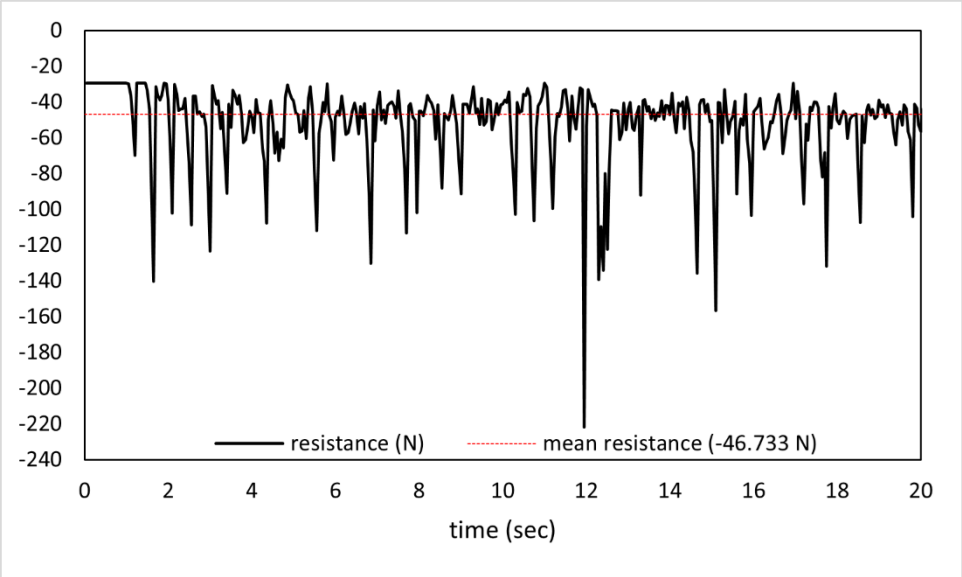

Fig. 5.4. Simulated time history of ice resistance at the surge speed of 0.3 m/s.

In Fig. 5.4, it can be noted that the ice resistance fluctuates around a mean value, which would be the resistance the ship would experience traversing level ice. The mean resistance is relatively small compared to the peak values of the simulated forces. The peaks indicate the maximum value of the icebreaking force that causes the ice to break in flexure. The resistance due to ice buoyancy and clearing (or submergence) is mostly consistent. These constant forces are the reason the resistance does not drop to zero after breaking a cusp. The simulated mean resistance is close to the model test data shown in Fig. 5.5. However, a linear relationship between mean resistance and ship speed can be observed in simulations, while model tests do not show a similar relationship.

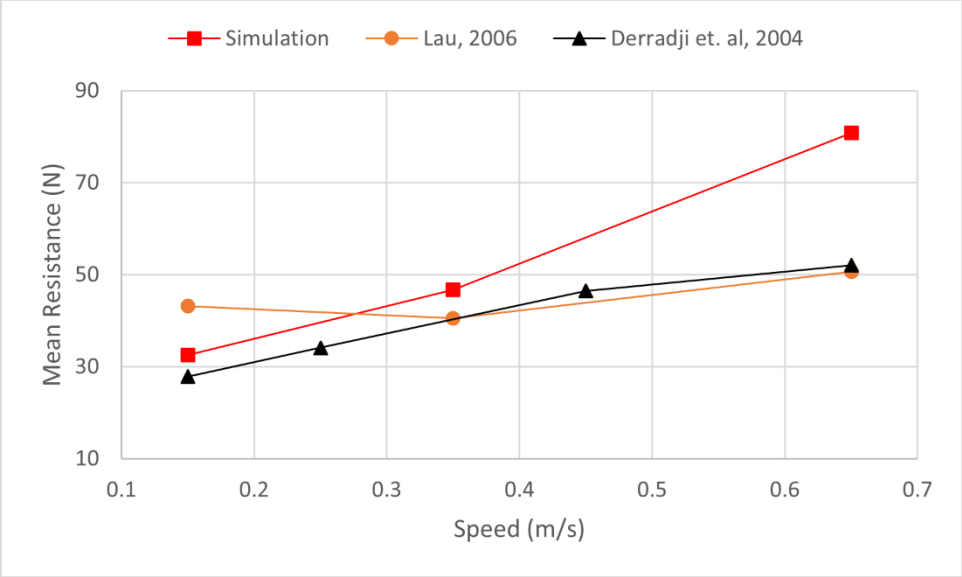

Fig. 5.5. Mean straight motion ice resistance for Model-scale Terry Fox.

5.3 CCGS Sir John Franklin Full-Scale Sea Trials

According to [14], [20], the IOT R-Class model ship is a 1:20 scaled model of the CCGS Sir John Franklin (1979). In 2003, Sir John Franklin was converted into an Arctic research vessel and recommissioned as CCGS Amundsen [64]. The full-scale tests conducted in this thesis are based on the water outline of the scaled 1979-2003 model of the ship. The waterline profile of the model is shown in Fig. 5.6, and the principal dimensions of the model-scale CCGS Sir John Franklin are listed in Table 5.3. The full-scale model is based on the model scale data, adjusted to fit the principle dimensions of the full-scale CCGS Sir John Franklin, shown in Table 5.4.

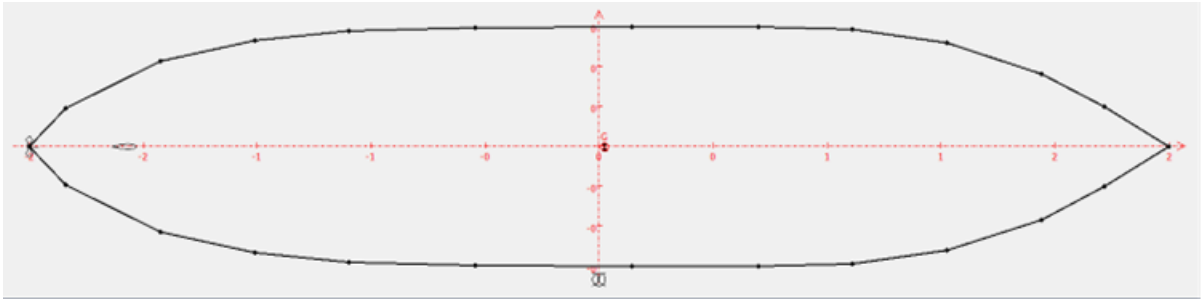

Fig. 5.6. Model-scale CCGS Sir John Franklin waterline profile (unit: m).

Table 5.3. Principal dimensions of the model-scale CCGS Sir John Franklin

Parameter	Notation	Value	Unit
Length	L	4.65	m
Breadth	B	0.96	m
Mass	M	965	kg
Draft	T	0.35	m
Block Coefficient	CB	0.611	N/A

This section presents the comparison between the simulation results and the sea trials data of a full-scale R-Class icebreaker, CCGS Sir John Franklin, in straight motion and turning a circle. The profile of the water line is the same as the model in Fig. 5.6, and the principal dimensions are listed in Table 5.4.

Table 5.4. Principal dimensions of the full-scale CCGS Sir John Franklin adapted from [14], [20].

Parameter	Notation	Value	Unit
Length Waterline	L_{WL}	96.52	m

Length between perpendiculars	L_{pp}	92.31	m
Breadth	B	19.5	m
Displacement	M	7720	t(kg)
Draft	T	7.0	m
Block Coefficient	CB	0.611	N/A

5.3.1 Straight Motion

Straight motion tests were conducted to validate the resistance obtained through the numerical method. Multiple free-running tests of full-scale CCGS Sir John Franklin are simulated in uniform level ice. The surge speeds in the tests range from 2.3 m/s to 6.3 m/s. All straight motion tests were simulated for 100 seconds. The ice conditions, listed in Table 5.5, and the mean resistances were obtained from [14], [36], [65].

Table 5.5. Ice mechanical properties for full-scale CCGS Sir John Franklin simulations adapted from [14], [20].

Parameter	Notation	Value	Unit
Flexural strength	σ_f	193-274	kPa
Crushing strength	p_0	1.3	MPa
Ice thickness	h_i	0.49-0.6	m
Young's modulus	E	1351-1918	MPa
Poisson ratio	ν	0.33	N/A
Friction coefficient	μ	0.1	N/A
Ice density	ρ_i	910	kg/m^3

Simplification Distance Tolerance	ϵ	0.02	-
-	C_f	2.2 [13]	-
-	C_v	-0.1 [13]	-

The mean resistance obtained from the numerical method proposed in this study is compared to sea trial data, and the results are contrasted in Fig. 5.7. Simulated mean surge resistance appears consistent with trial data, although slightly weaker. The difference is likely due to the inadequacy in recreating the environmental conditions encountered in the sea trials or fully modelling the vessel. The dip in mean resistance at the speed of 4.7 m/s is due to the lower recorded ice flexural strength of 193 kPA compared to 274 kPa at the speed of 4.6 m/s. An example of the generated broken ice track is shown in Fig. 5.8.

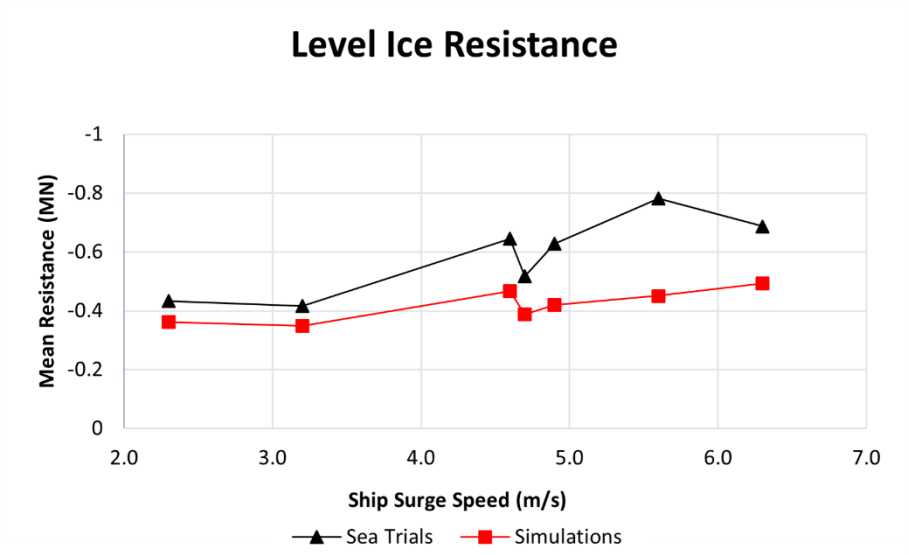

Fig. 5.7. Measured and simulated resistance for full-scale CCGS Sir John Franklin in straight motion.

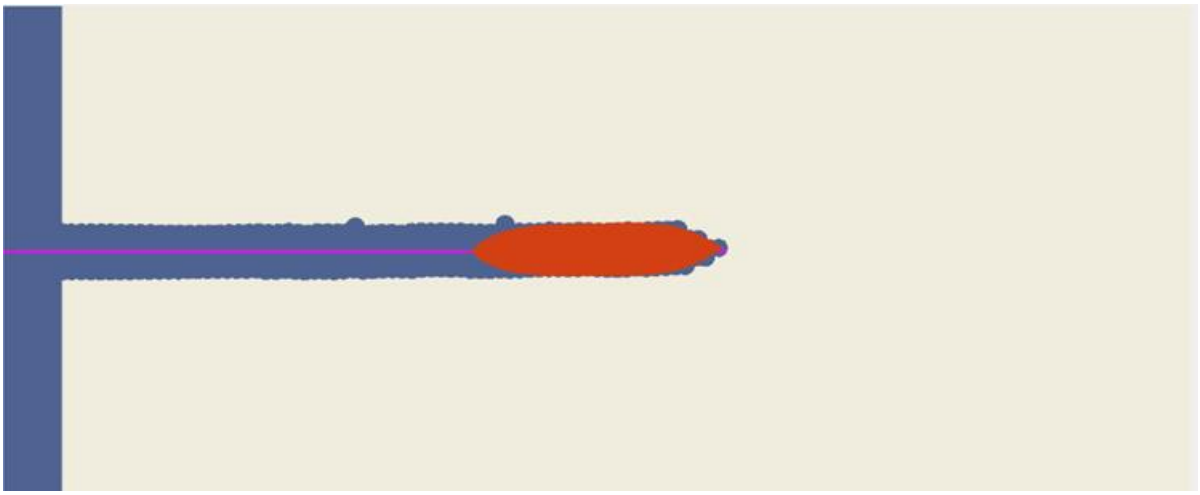

Fig. 5.8. Simulated ice track for full-scale CCGS Sir John Franklin in straight motion.

5.3.2 Turning Circle

The performance of CCGS Sir John Franklin turning in ice was also simulated. The tests were conducted with a 35° rudder (full-turn to starboard). The initial surge speed was 6.3 m/s with an engine shaft speed of 170 rpm. The ice track generated after a minute of simulation time is shown in Fig. 5.9. Agreement with the sea trial data could not be determined due to simulation constraints, detailed in the next section. However, the simulation result indicates that the numerical method is able to simulate some turning of the ship in level ice.

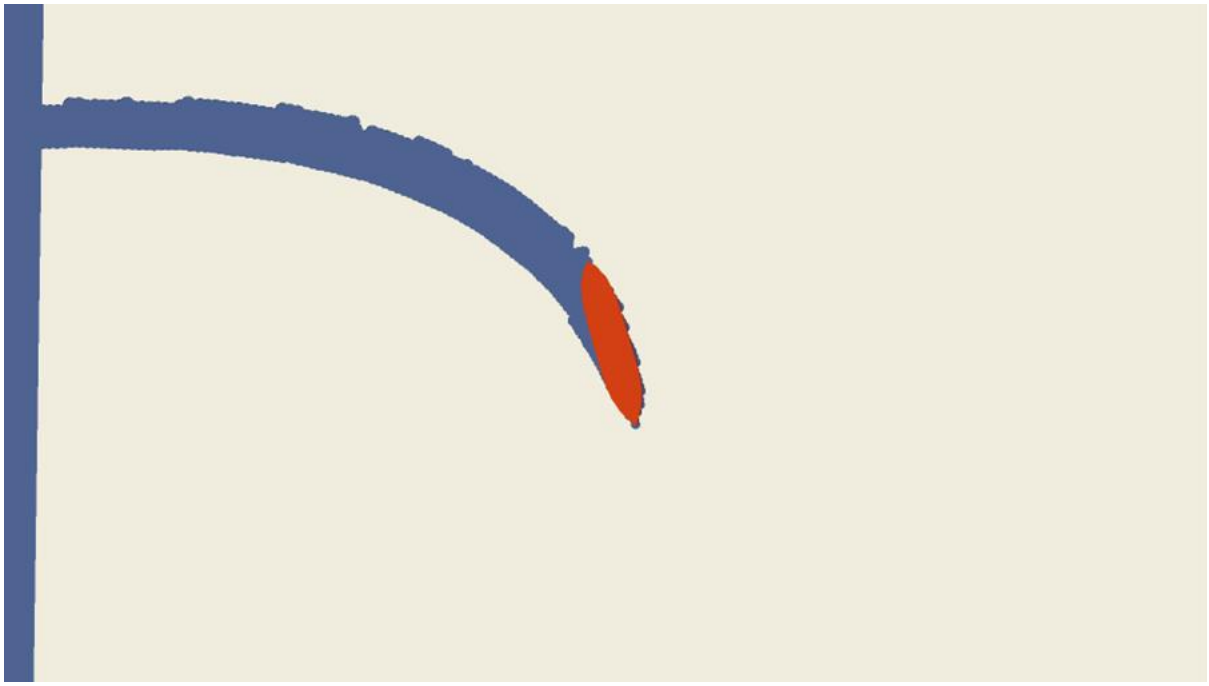

Fig. 5.9. Simulated half turning circle ice track for full-scale CCGS Sir John Franklin.

Due to the current state of GEM, it was not possible to conduct a full turning circle test in level ice. At the time of conducting this study, the guided navigation feature did not allow free turning, polygon portioning included frequent errors when computing the intersection, and the intermediate force vectors were not saved in a frame snapshot. Implementing these features was deemed out of the scope of this study. Therefore, the results presented in this section are for half a turning circle starting from open water. A 50 seconds sample of time history during the turning circle simulation is shown in Fig. 5.10, Fig. 5.11, and Fig. 5.12 for vessel velocity; and in Fig. 5.13, Fig. 5.14, and Fig. 5.15 for ice resistance.

Fig. 5.10 shows that the (forward) surge velocity of the ship drops during the turning circle test as a result of the ice resistance; meanwhile, the sway velocity and yaw rate increase in one direction due to the asymmetrical load on the bow of the ship, as shown in Fig. 5.11 and Fig. 5.12. This asymmetry can also be seen in surge force (Fig. 5.13) and sway force (Fig. 5.14) experienced by the ship during turning.

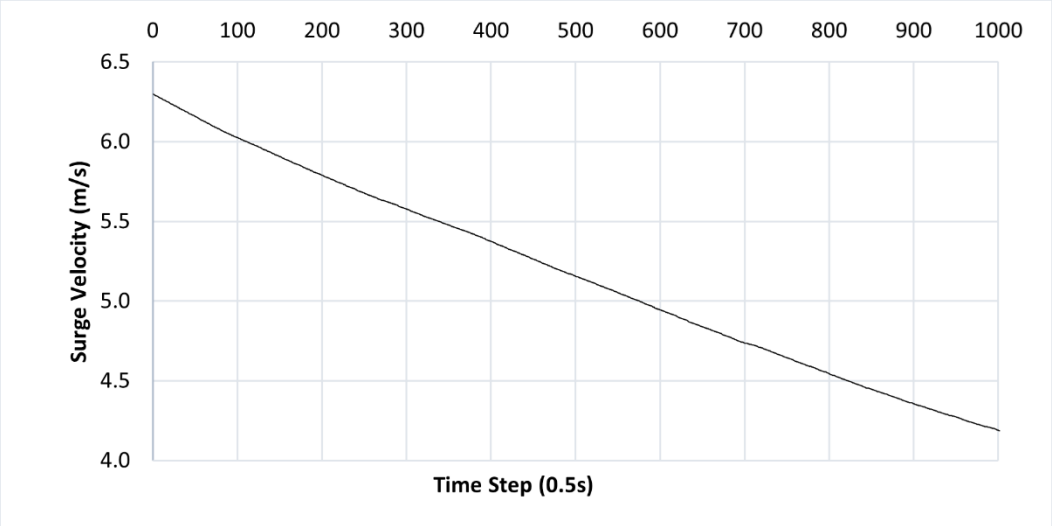

Fig. 5.10. Time history of surge velocity form the full-scale CCGS Sir John Franklin turning circle simulation.

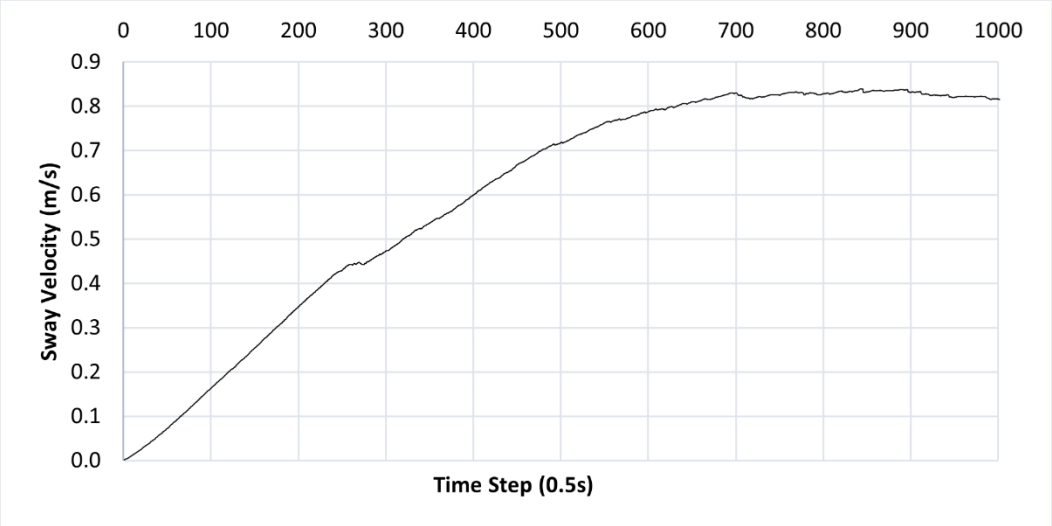

Fig. 5.11. Time history of sway velocity form the full-scale CCGS Sir John Franklin turning circle simulation.

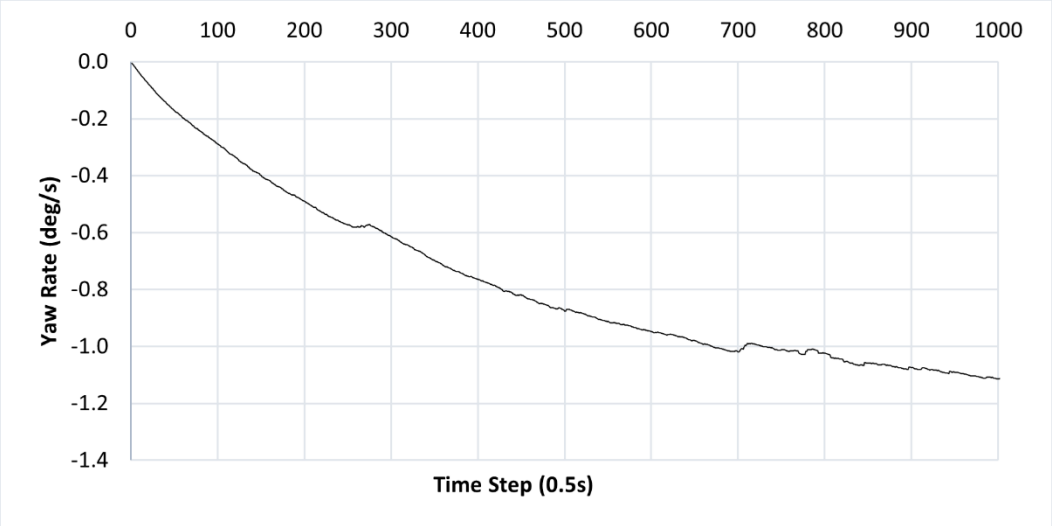

Fig. 5.12. Time history of yaw rate form the full-scale CCGS Sir John Franklin turning circle simulation.

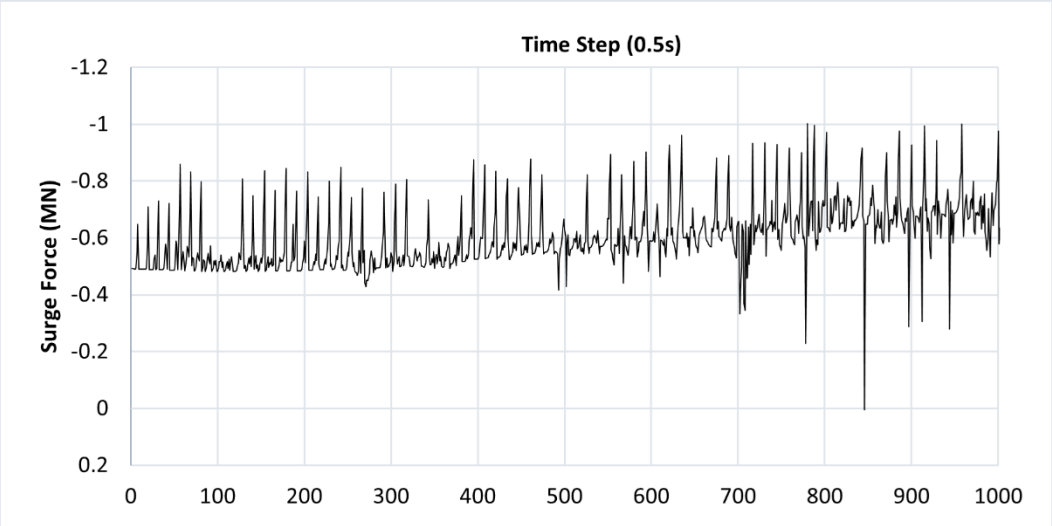

Fig. 5.13. Time history of surge force form the full-scale CCGS Sir John Franklin turning circle simulation.

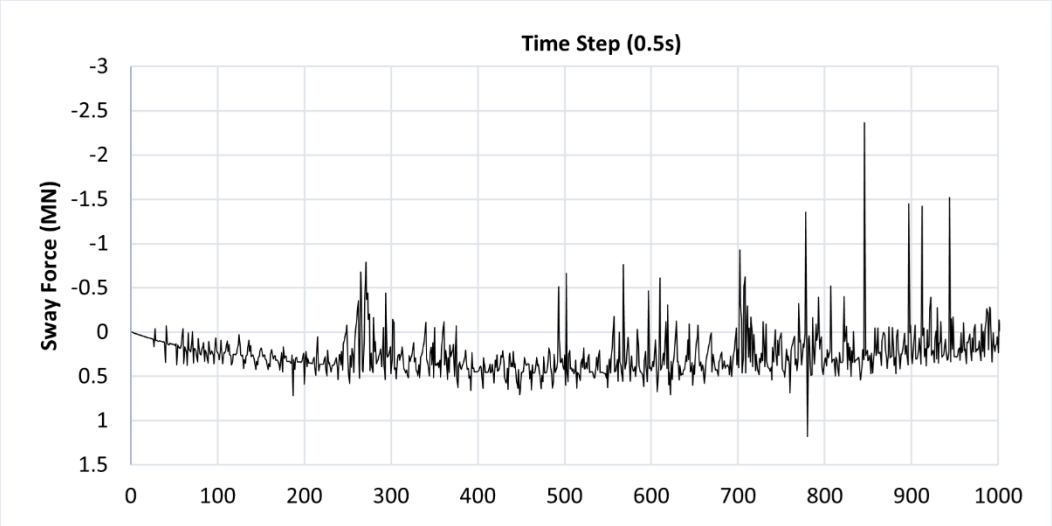

Fig. 5.14. Time history of sway force form the full-scale CCGS Sir John Franklin turning circle simulation.

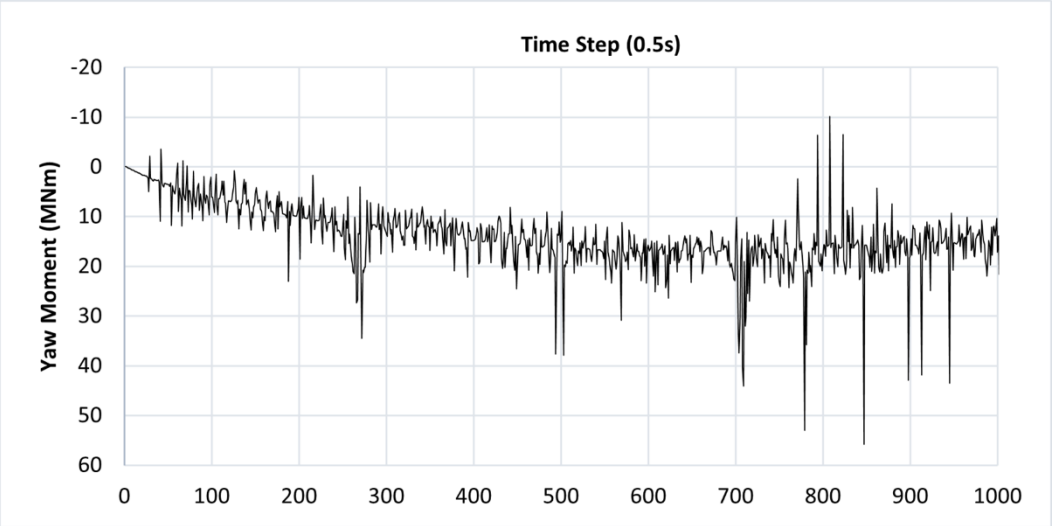

Fig. 5.15. Time history of yaw moment form the full-scale CCGS Sir John Franklin turning circle simulation.

5.4 Summary

This chapter presents the results of the validation tests conducted to compare the performance of the simulation with real-world data. The tests were carried out using one model ship and one full-scale ship. Good agreement is found between the output obtained through the numerical method and the data from full-scale and model-scale studies. The initial findings confirm the validity of using the method developed in this study to predict the performance of vessels traversing level ice and planning ice management operations. However, future development is needed to simulate a complete mission due to current simulation constraints.

Chapter 6: Conclusions and Recommendations

This thesis provides a hybrid, numerical and semi-empirical model that predicts ship-ice interaction in level ice environments. Furthermore, the model was integrated into an existing software solution, allowing for the simulation of ice management operations and vessel control in level ice.

6.1 Contributions

The contribution of this study can be broken down as follows:

- A literature review of analytical and numerical solutions for the problem of ship-ice interaction previously proposed in the literature.
- A modified ship-ice collision detection method in 2D that supports the continuous level ice breaking process is developed. The new method is based on the Polygon-Point Algorithm, allows for accurate collision detection in level ice, and offers an acceptable compromise between accuracy and performance.
- A revised mathematical model that describes the effect of ice submergence resistance on sway and yaw motions during turning in ice is derived. The model predicts ship motion based on hull geometry and interaction forces. Combined with numerically-obtained 3DOF ice breaking force, this study develops a comprehensive 2D level ice resistance model.
- A new method is proposed for calculating the contribution of broken ice to the submergence component of ice resistance. Previous research discarded broken floes and entirely depended on semi-empirical formulas to estimate the contribution of rubble ice to total ice resistance. Ice submergence contribution is calculated by numerically

deducting the ship-broken ice contact and solving for the forces generated by that contact. The inclusion of rubble ice would allow for more robust ice management simulations in cases where accuracy is favoured over performance.

- The integration of polygon partitioning and simplification algorithms to facilitate the increase in ice shape complexity. The tessellation of ice polygons maintains the accuracy of ice collision detection with the irregular concave shapes generated by ice breaking. Noise smoothing algorithms are utilized to reduce the complexity of the concave polygons before partitioning. The smoothing maintains the most significant ice features while reducing the number of ice vertices and convex sub-polygons. Thus, higher performance is achieved while maintaining engineering accuracy.
- The provided model is integrated into a simulation software program (GEM). The GEM software implementation of the model is able to simulate straight motion, turning, and guided motion in ice. Moreover, it is also capable of simulating ice management scenarios in level ice or open pack ice.
- The validation of the model is carried out using the Terry Fox model-scale data and the full-scale CCGS Sir John Franklin icebreaker trials. Multiple straight motion, turning, and self-propulsion simulations are conducted and compared with available published data.

6.2 Recommendations for Future Work

The model developed in this thesis is concerned with only a limited subsection of the ship-ice interaction and ice management problems. Therefore, to develop a more comprehensive model, further studies are recommended to explore the following:

- Empirical formulas are utilized for estimating the ice-induced forces, ice bearing capacity, and cusp size with a numerical solution for the collision geometry. Future work should explore replacing these formulas with numerical solutions. The inclusion of machine learning algorithms to reduce computation complexity, for example, the method proposed in [15], is a promising proposition. Machine learning algorithms could be trained on FEA data to provide a mapping between numerical collision detection and an FEA solution that predicts the forces generated from these contact scenarios. The trained model could be considered a portable, compressed FEA solution. Thus, providing accuracy beyond what is attainable by semi-empirical formulas without compromising performance.

- The proposed mathematical model expects that ice polygons are sufficiently larger than ice breaking vessels such that the ice plate could be assumed to be semi-infinite. In addition, ice properties, such as thickness and strength, are assumed to be uniform over the entire ice sheet. These assumptions do not match observations in operating environments or even controlled model-scale experiments. The change in breaking patterns due to ice plate size and local variations in ice properties should be further investigated.

- This study only considers ship movement in 3DOF. The current framework of GEM is 2D. The motions of surge, sway, and yaw are investigated for level ice breaking, while pitch, heave, and roll are considered out of scope. More research should be conducted in order to investigate ship motion in 6DOF and develop a full 3D model for ice breaking in GEM.

- The software does not reliably support multiple vessels per level ice sheet. The collision algorithm is capable of detecting multiple contacts and failure events per interaction.

Moreover, GEM supports simulations with multiple running vessels. However, this implementation assumes that only one vessel is traversing a level ice sheet at any time step. Support for simultaneous, multiple-vessel ice breaking events would allow for a broader range of ice management scenarios and rescue operations. The implementation of the aforementioned feature should be investigated for future software development.

- The provided algorithm is mainly sequential. Although GEM supports parallel execution on multiple computation cores, it primarily depends on a grid method where grid blocks are assigned to different threads. As this model was developed with the assumption of one vessel per ice sheet, it does not run efficiently under the multithreading design of GEM. The impact on performance is most notable with numerical ice submergence resistance turned on during simulations. Leveraging the advancements in data-driven parallel computing technology would benefit future level ice breaking software solutions as most computations are done on the small-scale sub-polygons and broken ice polygons.

- Polygon shapes grow in complexity with each breaking event. As a vessel progresses through the ice polygon, more convex sub-polygons are generated to represent the geometry. The provided software implementation includes a noise-reduction algorithm. However, the algorithm arbitrarily removes points with high deviance. In addition, the algorithm can generate triangles so thin or small that floating-point rounding errors cause collision detection glitches. Future work could utilize an intelligent algorithm capable of simplifying ice polygons while maintaining the minimum number of features required for simulation accuracy.

- The accuracy of ship-ice interaction models utilized in GEM is only guaranteed in an environment that has either exclusively level ice interaction events or exclusively open

pack ice interaction events, as currently, GEM cannot run in both modes simultaneously. In real-world scenarios, ship-ice interactions are not limited to one of these categories. More effort should be made in order to incorporate these two categories of ice models in GEM.

- Ice floes do not consistently break in a repeatable pattern. For example, ice cusps could overlap, which ought to result in a different breaking behaviour that is currently missing. In addition, thinner ice floes often split and are cleared. Some studies, such as [42], attempt to integrate multiple categories of simplified ice failure models. However, further research into integrating them into a numerical level ice breaking solution is required.

Bibliography

[1] S. J. Jones, “Ships in ice - a review,” *25th Symposium on Naval Hydrodynamics*, no. August, pp. 8–13, 2004, [Online]. Available: http://nparc.cisti-icist.nrc-cnrc.gc.ca/eng/view/object/?id=2bb7fdef-1187-413f-a0ab-2ad2204218ff

[2] R. Runeberg, “On steamers for winter navigation and ice-breaking. (Including plates at back of volume),” *Minutes of the Proceedings of the Institution of Civil Engineers*, vol. 97, no. 1889, pp. 277–301, 1889, doi: 10.1680/imotp.1889.20763.

[3] E. Enkvist, *On the ice resistance encountered by ships operating in the continuous mode of icebreaking*. Helsinki: Swedish Academy of Engineering Sciences in Finland Helsinki, 1972.

[4] V. Kastelyan, I. Poznyac, and A. Ryvlin, “Ice resistance to motion of a ship,” *Sudostroenie*, p. 238, 1968.

[5] J. W. Lewis and R. Y. Edwards Jr, “Methods for predicting icebreaking and ice resistance characteristics of icebreakers,” in *Transactions of the Society of Naval Architects and Marine Engineers*, 1970, vol. 78, pp. 213–249.

[6] V. R. Milano, “Ship resistance to continuous motion in ice,” in *Transactions of the Society of Naval Architects and Marine Engineers*, 1973, vol. 81, pp. 274–306.

[7] T. v. Kotras, A. v. Baird, and J. N. Naegle, “Predicting ship performance in level ice,” in *Transactions of the Society of Naval Architects and Marine Engineers*, 1984, vol. 91, pp. 329–349.

[8] G. Lindqvist, “A straightforward method for calculation of ice resistance of ships,” in *International Conference on Port and Ocean Engineering under Arctic Conditions*, 1989, vol. 1, pp. 722–735.

[9] K. Riska, M. Wilhelmson, K. Englund, and T. Leiviskä, “Performance of merchant vessels in ice in the Baltic (Research Report No. 52),” Espoo, Finland, 1997. [Online]. Available: traficom.fi/sites/default/files/10730-No_52_Performance_of_merchant_vessels_in_ice_in_the_Balt.pdf

[10] P. Valanto, “The resistance of ships in level ice,” in *Transactions of the Society of Naval Architects and Marine Engineers*, 2001, vol. 109, pp. 53–83.

[11] B. Su, K. Riska, and T. Moan, “A numerical method for the prediction of ship performance in level ice,” *Cold Reg Sci Technol*, vol. 60, no. 3, pp. 177–188, 2010, doi: 10.1016/j.coldregions.2009.11.006.

[12] R. Lubbad and S. Løset, “A numerical model for real-time simulation of ship-ice interaction,” *Cold Reg Sci Technol*, vol. 65, no. 2, pp. 111–127, 2011, doi: 10.1016/j.coldregions.2010.09.004.

[13] Q. Zhou, H. Peng, and W. Qiu, “Numerical investigations of ship-ice interaction and maneuvering performance in level ice,” *Cold Reg Sci Technol*, vol. 122, pp. 36–49, 2016, doi: 10.1016/j.coldregions.2015.10.015.

[14] D. Spencer and S. J. Jones, “Model-scale/Full-scale correlation in open water and ice for canadian coast guard ‘r-class’ icebreakers,” *Journal of Ship Research*, vol. 45, no. 4, pp. 249–261, 2001, doi: 10.5957/jsr.2001.45.4.249.

[15] F. Li, F. Goerlandt, and P. Kujala, “Numerical simulation of ship performance in level ice: A framework and a model,” *Applied Ocean Research*, vol. 102, p. 80 + app. 84, 2020, doi: 10.1016/j.apor.2020.102288.

[16] P. Valanto, “Experimental study of the icebreaking cycle in 2-D,” in *Proceedings of the International Offshore Mechanics and Arctic Engineering Symposium*, 1989, vol. 4, no. 8, pp. 343–349.

[17] C. Daley, “Ice edge contact a brittle failure process model,” in *Acta Polytechnica Scandinavica, Mechanical Engineering Series*, 1991, no. 100, p. 92.

[18] Z. Liu, J. Amdahl, and S. Løset, “Integrated numerical analysis of an iceberg collision with a foreship structure,” *Marine Structures*, vol. 24, no. 4, pp. 377–395, 2011, doi: 10.1016/j.marstruc.2011.05.004.

[19] P. Valanto, “Theoretical investigation of the icebreaking cycle in 2-D,” in *Proceedings of the 9th International Offshore Mechanics and Arctic Engineering Symposium*, 1990, pp. 111–126.

[20] J. Liu, “Mathematical modeling ice-hull interaction for real time simulations of ship manoeuvring in level ice (Doctoral thesis),” Memorial University of Newfoundland and Labrador, 2009.

[21] W. Lu, S. Løset, and R. Lubbad, “Ventilation and backfill effect during ice-sloping structure interactions,” in *21st IAHR International Symposium on Ice*, 2012, pp. 826–841.

[22] X. Tan, K. Riska, and T. Moan, “Effect of dynamic bending of level ice on ship’s continuous-mode icebreaking,” *Cold Reg Sci Technol*, vol. 106–107, pp. 82–95, 2014, doi: 10.1016/j.coldregions.2014.06.011.

[23] Y. Xue, R. Liu, Z. Li, and D. Han, “A review for numerical simulation methods of ship–ice interaction,” *Ocean Engineering*, vol. 215, p. 107853, Nov. 2020, doi: 10.1016/j.oceaneng.2020.107853.

[24] J. Blanchette and M. Summerfield, “C++ GUI programming with Qt 4,” 2008. http://portal.acm.org/citation.cfm?id=1406186 (accessed Jan. 31, 2021).

[25] M. Segal, K. Akeley, C. Frazier, and J. Leech, “The OpenGL graphics system: A specification (version 4.6),” 2019. https://www.khronos.org/registry/OpenGL/specs/gl/glspec46.core.pdf (accessed Jan. 31, 2021).

[26] S. Alawneh, R. Dragt, D. Peters, C. Daley, and S. Bruneau, “Hyper-Real-Time Ice Simulation and Modeling Using GPGPU,” *IEEE Transactions on Computers*, vol. 64, no. 12, pp. 3475–3487, 2015, doi: 10.1109/TC.2015.2409861.

[27] Y. N. Popov, O. v Faddeev, D. E. Kheisin, and A. A. Yakovlev, “Strength of ships sailing in ice,” Sudostroyeniye Publishing House, Technical Translation by U.S. Army Foreign Science and Technology Center, Leningrad, 1967.

[28] C. Daley, S. Alawneh, D. Peters, and B. Colbourne, “GPU-Event-Mechanics evaluation of ice impact load statistics,” in *Arctic Technology Conference*, 2014, pp. 809–819. doi: 10.4043/24645-ms.

[29] C. Daley, S. Alawneh, D. Peters, B. Quinton, and B. Colbourne, “GPU modeling of ship operations in pack ice,” in *International Conference and Exhibition on Performance of Ships and Structures in Ice 2012, ICETECH 2012*, 2012, pp. 122–127.

[30] D. B. Colbourne, “A three component method of analyzing icebreaking resistance,” Memorial University of Newfoundland Labrador, 1989.

[31] Y. A. Shimanskii, “Conditional standards of ice qualities of a ship, Trans. Arctic Research Institute, Northern Sea Route Administration Publishing House,” Translation T-381-01 by Engineering Consulting and Translation Center (ECTC), Leningrad, 1938.

[32] J.-E. Jansson, “Ice-breakers and their design,” *European Shipbuilding*, vol. 5, pp. 112–128, 1956.

[33] E. Enkvist, “A survey of experimental indications of the relation between the submersion and breaking components of level ice resistance to ships,” in *International Conference on Port and Ocean Engineering under Arctic Conditions*, 1983, vol. 27, pp. 484–493.

[34] C. Daley, *Sea Ice Engineering for Ships and Offshore Structures*, 10f ed. 2020. [Online]. Available: https://www.engr.mun.ca/~cdaley/8074/IceTextv10j.pdf

[35] D. Spencer, F. M. Williams, S. T. Mathews, and I. Bayly, “Full scale trials in level ice with Canadian R-class icebreaker,” in *Transactions of the Society of Naval Architects and Marine Engineers*, 1992, vol. 100.

[36] Q. Zhou, “Numerical simulation for ship manoeuvring and path following in level ice,” Memorial University of Newfoundland and Labrador, 2014.

[37] M. Lau, K. P. Lawrence, and L. Rothenburg, “Discrete element analysis of ice loads on ships and structures,” *Ships and Offshore Structures*, vol. 6, no. 3, pp. 211–221, 2011, doi: 10.1080/17445302.2010.544086.

[38] D. T. Nguyen, A. H. Sørbø, and A. J. Sørensen, “Modelling and control for dynamic positioned vessels in level ice,” in *IFAC Proceedings Volumes (IFAC-PapersOnline)*, 2009, vol. 42, no. 18. doi: 10.3182/20090916-3-BR-3001.0006.

[39] D. H. Nguyen, D. T. Nguyen, S. T. Quek, and A. J. Sørensen, “Position-moored drilling vessel in level ice by control of riser end angles,” *Cold Reg Sci Technol*, vol. 66, no. 2–3, pp. 65–74, 2011, doi: 10.1016/j.coldregions.2011.01.007.

[40] J. Sawamura, K. Riska, and T. Moan, “Numerical simulation of breaking patterns in level ice at ship’s bow,” in *Proceedings of the International Offshore and Polar Engineering Conference*, 2009, pp. 600–607.

[41] J. Sawamura, “Numerical Investigation of Ice Bending Failure and Ice Submerging Force for Ship Maneuvering in Level Ice,” *21st IAHR International Symposium on Ice*, 2012.

[42] J. Sawamura, “2D numerical modeling of icebreaker advancing in ice-covered water,” *International Journal of Naval Architecture and Ocean Engineering*, vol. 10, no. 3, pp. 385–392, 2018, doi: 10.1016/j.ijnaoe.2018.02.005.

[43] S. Wang, “A dynamic model for breaking pattern of level ice by conical structures,” *Acta Polytechnica Scandinavica, Mechanical Engineering Series*, vol. 156, p. 120, 2001.

[44] C. Daley, J. Tuhkuri, and K. Riska, “The role of discrete failures in local ice loads,” *Cold Reg Sci Technol*, vol. 27, no. 3, 1998, doi: 10.1016/S0165-232X(98)00007-X.

[45] M. Lau, J. C. Liu, A. Derradji-aouat, and F. M. Williams, “Preliminary Results of Ship Maneuvering in Ice Experiments Using a Planar Motion Mechanism,” *17th IAHR International Symposium on Ice*, no. June, 2004.

[46] J. Sawamura, S. Kioka, and A. Konno, “Experimental and numerical investigation on ice submerging for icebreaker with 2D model test using synthetic ice,” in *Proceedings of the International Conference on Port and Ocean Engineering under Arctic Conditions, POAC*, 2015, vol. 2015-January.

[47] J. Sawamura, Y. Yamauchi, and K. Anzai, “Simulation of ice force and breaking pattern for icebreaking ship in level ice,” in *Proceedings of the International Conference on Offshore Mechanics and Arctic Engineering - OMAE*, 2017, vol. 8. doi: 10.1115/OMAE2017-61583.

[48] Q. Zhou and H. Peng, “Numerical simulation of a dynamically controlled ship in level ice,” *International Journal of Offshore and Polar Engineering*, vol. 24, no. 03, pp. 184–191, 2014.

[49] D. Eberly, “Intersection of Convex Objects: The Method of Separating Axes,” 2008.

https://www.geometrictools.com/Documentation/MethodOfSeparatingAxes.pdf (accessed Jan. 31, 2021).

[50] G. T. Toussaint, “A simple linear algorithm for intersecting convex polygons,” *Vis Comput*, vol. 1, no. 4, 1985, doi: 10.1007/BF01898355.

[51] J. Fernández, L. Cánovas, and B. Pelegrín, “Algorithms for the decomposition of a polygon into convex polygons,” *Eur J Oper Res*, vol. 121, no. 2, 2000, doi: 10.1016/S0377-2217(99)00033-8.

[52] C. Daley, A. Kendrick, and B. Quinton, “Safe Speeds in Ice (BMT Report 6931DFR.Rev00),” 2011.

[53] A. D. Kerr, “The Bearing Capacity of Floating Ice Plates Subjected to Static or Quasi-Static Loads,” *Journal of Glaciology*, vol. 17, no. 76, 1976, doi: 10.1017/s0022143000013575.

[54] R. L. Graham, “An efficient algorithm for determining the convex hull of a finite planar set,” *Inf Process Lett*, vol. 1, no. 4, pp. 132–133, Jun. 1972, doi: 10.1016/0020-0190(72)90045-2.

[55] M. Duckham, L. Kulik, M. Worboys, and A. Galton, “Efficient generation of simple polygons for characterizing the shape of a set of points in the plane,” *Pattern Recognit*, vol. 41, no. 10, 2008, doi: 10.1016/j.patcog.2008.03.023.

[56] M. Keil and J. Snoeyink, “On the time bound for convex decomposition of simple polygons,” *Int J Comput Geom Appl*, vol. 12, no. 3, 2002, doi: 10.1142/S0218195902000803.

[57] S. Hertel and K. Mehlhorn, “Fast triangulation of the plane with respect to simple polygons,” *Information and Control*, vol. 64, no. 1–3, pp. 52–76, Jan. 1985, doi: 10.1016/S0019-9958(85)80044-9.

[58] M. de Berg, O. Cheong, M. van Kreveld, and M. Overmars, *Computational geometry: Algorithms and applications*. 2008. doi: 10.1007/978-3-540-77974-2.

[59] U. Ramer, “An iterative procedure for the polygonal approximation of plane curves,” *Computer Graphics and Image Processing*, vol. 1, no. 3, 1972, doi: 10.1016/S0146-664X(72)80017-0.

[60] D. H. Douglas and T. K. Peucker, “Algorithms for the Reduction of the Number of Points Required to Represent a Digitized Line or Its Caricature,” *Cartographica: The International Journal for Geographic Information and Geovisualization*, vol. 10, no. 2, 1973, doi: 10.3138/fm57-6770-u75u-7727.

[61] J. E. Hershberger and J. Snoeyink, “Speeding up the Douglas-Peucker line-simplification algorithm,” *Proc. 5th Intl. Symp. on Spatial Data Handling*, 1992.

[62] A. Derradji-Aouat and A. van Thiel, “Terry Fox resistance tests - Phase III (PMM) ITTC Experimental Uncertainty Analysis Iniative,” National Research Council of Canada. Institute for Ocean Technology, St. John’s, NL, 2004. doi: 10.4224/8896297.

[63] M. Lau, “Preliminary modelling of ship manoeuvring in ice using a PMM,” National Research Council of Canada. Institute for Ocean Technology, St. John’s, Newfoundland, 2006. doi: 10.4224/8895076.

[64] Canadian Coast Guard, “CCGS Amundsen,” 2022. https://inter-j01.dfo-mpo.gc.ca/fdat/vessels/3 (accessed Mar. 31, 2022).

[65] A. Keinonen, “Icebreaker characteristics synthesis; Volume I, Main report,” 1996.